localized in the nucleus (Fig. 1c, d). Although a kinase-negative mutant (NLK^{K155M}) was located in the nucleus (Fig. 1d), this mutant lost transrepressive activity for PPAR-γ (Fig. 1b).

CaMKII (calcium/calmodulin-dependent protein kinase II) is an upstream factor of TAK1–TAB2 that activates NLK for its repressive activity[20]. Treatment with KCl, which activates CaMKII, was effective in repressing PPAR-γ function (Fig. 1e). A constitutively kinase-dead form of CaMKII (CaMKII KD) and the CaMKII inhibitor KN93 abrogated the suppressive activity of NLK for PPAR-γ (Fig. 1e). Through investigating membrane-receptor ligand candidates that activate NLK in ST2 cells, we found that Wnt-5a mediated the suppressive function of NLK (Fig. 1f). However, Wnt-5a action was not abrogated by knockdown of β-catenin (Fig. 1f) and, unlike Wnt-3a, Wnt-5a did not activate the TCF-LEF-mediated canonical cascade (Fig. 1g).

An activated non-canonical Wnt cascade attenuates adipogenesis through repression of PPAR-γ activity

Expression of Wnt ligands and their receptors was tested in ST2 cells. ST2 cells are derived from mouse bone marrow stromal cells and differentiate into either adipocytes through PPAR-γ activation or osteoblasts if induced by several cytokines[15]. We observed that Wnt-5a and several frizzled receptor genes are expressed at significant levels in ST2 cells as well as in mouse bone marrow cell primary culture (data not shown).

Wnt-5a, but not the canonical Wnt ligand Wnt-3a, was capable of repressing PPAR-γ function through NLK on synthetic (Fig. 1f) as well as natural PPAR-γ target gene promoters (see Supplementary Information, Fig. S1a). $TAK1^{K63W}$ (a kinase-dead mutant of MAPKKK), CaMKII KN as well as NLK^{K155M} abrogated Wnt-5a-induced suppression of PPAR-γ (Fig. 1h). Furthermore, knockdown of NLK (see Supplementary Information, Fig. S2) abolished the effect of Wnt-5a, CaMKII and TAK1–TAB2 (Fig. 1b, e, f). Transactivation functions of adipogenic (CCAAT/enhancer binding protien (C/EBPβ), glucocorticoid (GR)) or osteoblastogenic (Runx2) transcriptional factors were not modulated by Wnt-5a treatment (Fig. 1i). It is notable that the activated non-canonical Wnt signalling by Wnt-5a lowered the basal activity of the tested PPAR-γ target gene promoters (see Fig. 1h for instance). Interestingly, PPAR-γ phosphorylation mutants (PPAR-γ S8A, S112A and S8A-S112A), which have been reported to be insensitive to MAPK (ERK)-induced suppression[14], remained susceptible to the suppressive action of NLK (see Supplementary Information, Fig. S1b).

Wnt-5a has been identified as a potential genetic determinant of diet-induced obesity[27] and so we examined the effect of Wnt-5a on ST2 cell differentiation. Treatment with Tro induced adipogenesis, lipid accumulation and glycerol-3-phosphate dehydrogenase (GPDH) activity (Fig. 2a, c) as reported previously[15,28]. Under these conditions, Wnt-5a seemed to mediate transdifferentiation of adipo-progenitors into osteoblastic cells expressing alkaline phosphatase (ALP) (Fig. 2a, c), as reflected by expression of markers of mature adipocytes (GPDH, aP2 and LXR-α) and osteoblasts (ALP and Runx2) (Fig. 2d and Supplementary Information, Fig. S1c), but not chondrocyte-specific markers (type II collagen and aggrecan) (Fig. 2e). Knockdown of β-catenin by RNA interference (RNAi) did not abrogate Wnt-5a-induced adipogenesis inhibition (Fig. 2b, c). Again, this supports the involvement of the non-canonical Wnt cascade activated by Wnt-5a in promoting osteoblastogenesis through attenuating adipogenesis with induction of Runx2, a critical osteoblastogenic transcription factor (Fig. 2d and Supplementary Information, Fig. S1c). Although TAZ (transcriptional co-activator with PDZ-binding motif) has recently been identified as an osteoblastogenic factor of mesenchymal stem-cell differentiation by repressing PPAR-γ function[29], TAZ seemed to be independent from the mechanism of Wnt-5a-induced suppression of the transactivation function of PPAR-γ (see Supplementary Information, Fig. S3a), and also independent from adipogenesis inhibition (see Supplementary Information, Fig. S3b). Together with the observation that *TAZ* gene expression is unaltered by Wnt-5a treatment (see Supplementary Information, Fig. S3c), we assume that the TAZ-mediated cascade does not converge with that of Wnt-5a in the differentiation of mesenchymal stem cells. Thus, activated PPAR-γ seems to potentiate cytodifferentiation of mesenchymal stem cells into adipo- or osteo-progenitors.

Wnt-5a haploinsufficiency in mice induces bone loss with enhanced adipogenesis in bone marrow

As expected from the physiological effect of PPAR-γ on adipogenesis from mesenchymal stem cells in bone marrow[30], haploinsufficiency of PPAR-γ in mice ($PPAR\text{-}\gamma^{+/-}$) resulted in a reduction of adipocytes in bone marrow (Fig. 3b, c). Moreover, as expected from *in vitro* observations, bone mass increase, presumably because of increased osteoblastogenesis from bone marrow stem cells, was observed in $PPAR\text{-}\gamma^{+/-}$ male mice[31] (Fig. 3a, b, e). By contrast, $Wnt\text{-}3a^{+/-}$ males[32] exhibited bone loss (Fig. 3a, b, d, e), consistent with previous reports that canonical Wnt signalling is responsible for bone formation through stimulating osteoblastogenesis[33–35]. However, unlike $PPAR\text{-}\gamma^{+/-}$ mice, adipogenesis seemed unaffected in $Wnt\text{-}3a^{+/-}$ mice (Fig. 3b), suggesting that canonical Wnt signalling is unlikely to attenuate adipogenesis from adipo- or osteo-progenitor cells.

Supporting *in vitro* observations of Wnt-5a action, $Wnt\text{-}5a^{+/-}$ mice[36] showed a clear bone-loss phenotype, with decreased trabecular bone mass (Fig. 3d, and see arrow heads of Fig. 3e). Presumably, this was caused by reduced osteoblastogenesis as shown in the femur (Fig. 3a), which shows significantly elevated number of adipocytes in bone marrow (Fig. 3b, c) when compared with wild-type littermates. Taken together, these findings confirm that Wnt-5a potentiates the cell-lineage decision of bone marrow mesenchymal stem cells into osteoblasts, presumably through the non-canonical Wnt signalling pathway.

NLK activated by Wnt-5a forms a complex with a HKMT

We then tested whether NLK-induced suppression of PPAR-γ function was linked to HDAC using the HDAC inhibitor, tricostatin A (TSA). However, TSA was unable to reverse NLK-mediated suppression of PPAR-γ function in ST2 cells (Fig. 4a). No alteration in PPAR-γ protein turnover was detected even when NLK was overexpressed (see Supplementary Information, Fig. S4a). Considering that NLK is a downstream factor of activated Wnt-5a (ref. 20), we reasoned that NLK might associate with unknown co-regulators to suppress PPAR-γ function. We therefore biochemically purified NLK-containing complexes from nuclear extracts of KCl-treated HeLa cells expressing Flag-tagged NLK by two-step purification[37,38] (Fig. 4b). We identified an NLK–nuclear-protein complex with a molecular weight of around 400–500 kDa by using glycerol gradient centrifugation fractionation (Fig. 4c). By MALDI-TOF mass spectrometric analysis of the other two complex components, two proteins (220 kDa and 170 kDa) were identified. The 220-kDa band was a DEXH-box and CHD-domain-containing ATPase protein, CHD7

(ref. 24). The 170-kDa band was an HKMT (SETDB1) that suppresses transcription through histone H3 methylation at K9 (refs 22, 23). We confirmed the formation of these complexes by a two-step immunoprecipitation assay (Fig. 4d) and association of endogenous NLK, SETDB1 and CHD7 in a complex with PPAR-γ was only detectable after treatment with Wnt-5a in ST2 cells (Fig. 4e). This Wnt-5a-induced association was abrogated when NLK, SETDB or CHD7 was knocked down by RNAi (Fig. 4f). In a GST pull-down assay, CHD7 seemed to be able to physically interact with NLK, SETDB1 and PPAR-γ, whereas PPAR-γ did not interact with SETDB1 (Fig. 4g). However, PPAR-γ seemed to associate with SETDB1 in the presence of CHD7 (Fig. 4g; lower panel).

SETDB1 T976A phosphorylation by NLK is a prerequisite for HKMT activity and transrepression of PPAR-γ

We hypothesized that Wnt-5a-activated NLK phosphorylates SETDB1, because SETDB1 harbours several putative phosphorylation sites that could be NLK substrates (Fig. 5b). Using an anti-phosphorylated Ser–Thr antibody column, endogenous SETDB1 was found to be phosphorylated in a Wnt-5a-dependent manner (Fig. 5a). Wnt-5a-induced phosphorylation and repressive action on PPAR-γ was tested using SETDB1 deletion mutants (see Supplementary Information Fig. S4b). The mapped carboxy-terminal domain contains putative Thr–Ser phosphorylation site residues, and these were mutated to alanine (T700A, T754A, T976A, S1066A and S1277A; Fig. 5b). Among the five tested SETDB1 point mutants, only the T976A mutant was found to be deficient in SETDB1 repressive action (Fig. 5b) and was not phosphorylated by NLK either *in vivo* or *in vitro* (Fig. 5c, d). Interestingly, as a reflection of the importance of Thr976 phosphorylation for SETDB1 function, the region around Thr976 is highly conserved between human and mouse SETDB1 despite having only about 75% homology in adjacent regions (Fig. 5b). Significantly, Wnt-5a-induced complex formation of NLK–CHD7 with SETDB1 and PPAR-γ was abrogated by the T976A point mutation (Fig. 5e). The expected activity of the SETDB1 histone methyltransferase was detected in the NLK complex from Wnt-5a-treated ST2 cells (Fig. 5f). However, knockdown of either SETDB1 or CHD7 reduced the histone methyltransferase activity of the NLK complex (Fig. 5f), suggesting that SETDB1 requires assembly with NLK and CHD7 as a complex. Reflecting the presence of two chromodomains[39] in CHD7, CHD7 demonstrated physical interactions with tri-methylated H3-K4 and H3-K9 in a peptide pull-down assay and a histone-binding assay with semi-purified histones from HeLa cells (Fig. 5g). However, such preferential and significant interactions were not detected for acetylated H3.

Wnt-5a-induced H3-K9 methylation represses PPAR-γ-dependent activation of PPAR-γ target gene promoters

We then performed a chromatin immunoprecipitation (ChIP) analysis of endogenous transcriptional factors and histone modifications at the PPAR-γ binding site (PPRE) of the aP2 gene promoter[13]. Tro treatment induced recruitment of known PPAR-γ co-activator SRC-1 and co-repressor N-CoR (Fig. 6a). Treatment with Wnt-5a for 6 h in the presence of Tro induced recruitment of NLK, CHD7 and SETDB1 to the proximal PPRE region, but not to the other distal region on the aP2 gene promoter. Furthermore, consistent with SETDB1 recruitment, an increase in histone di- and tri-methylation at histone H3-K9 was observed together with hypoacetylation of histone H3 (Fig. 6a). Similar findings were also observed with the other PPAR-γ target gene (LXR-α) promoter (see Supplementary Information, Fig. S5b). Such coordinated histone modification to inactivate chromatin was more evident when ST2 cells were treated with Wnt-5a for 7 d to induce osteoblastogenesis (Fig. 6b). In comparison, histone H3-K9 on the Runx2 promoter was highly acetylated, and recruitment of neither PPAR-γ nor SETDB1 was seen in the same cells treated with Wnt-5a (Fig. 6c). These observations suggested that the Runx2 gene promoter is transcriptionally active in the presence of Wnt-5a, consistent with induction of the *Runx2* gene during Wnt-5a-induced osteoblastogenesis (Fig. 2d and see Supplementary Information, Fig. S1c).

Wnt-5-induced osteoblastogenesis from adipo- or osteoprogenitor cells requires NLK, SETDB1 and CHD7

With reference to these findings, we observed that overexpression of either NLK or SETDB1 was able to induce osteoblastogenesis rather than adipogenesis in ST2 cells (Fig. 7a, b; see Supplementary Information Fig. S2). Conversely, overexpression of an NLK mutant (NLK-KD) and SETDB1 mutants (SETDB1 T976A and ΔSET) and knockdown of NLK, SETDB1 or CHD7 induced adipogenesis rather than osteoblastogenesis even in the presence of Wnt-5a (Fig. 7a–d). Furthermore, these knockdowns abrogated the Wnt-5a-induced H3-K9 methylation and subsequent histone modification in the aP2 gene promoter (compare Fig. 6b with 7e).

DISCUSSION

Activated PPAR-γ is remarkably potent in cytodifferentiation, and several co-regulators of PPAR-γ, and cross-regulation by other cellular signalling pathways, have been previously described[10–12]. In particular, during PPAR-γ agonist-induced adipogenesis from bone marrow mesenchymal stem cells, activated PPAR-γ seems to function at multiple steps of the cytodifferentiation process. This is evident because bone marrow mesenchymal stem cells are pleiotropic and can differentiate into osteoblasts, chondrocytes or myoblasts depending on the activities of cell-lineage determinants[17].

In this study, we have found that Wnt-5a induces osteoblastogenesis through attenuating PPAR-γ-induced adipogenesis in mesenchymal stem cells of bone marrow. Wnt-5a activated a non-canonical Wnt signalling cascade mediated through CaMKII–TAK1–TAB2–NLK, but did not trigger the β-catenin–TCF canonical Wnt signalling pathway. Wnt signalling pathways have previously been described as being able to cross-talk with signalling pathways of certain NRs[40,41], and the pivotal roles of such cross-talk in cell-fate decisions have recently been verified in *Caenorhabditis elegans*[42]. This would suggest that such cross-regulation is conserved in metazoans. However, unlike the non-canonical Wnt cascade presented here, the canonical pathway mediated through β-catenin–TCF is known to co-activate the transactivation function of activated NRs including PPAR-γ (refs 40, 41). Thus, it is likely that Wnt ligands, in a positive or negative manner, modulate the functions of NRs in transcriptional control, depending on their specific downstream signalling cascades.

Osteoblastogenesis was induced by Wnt-5a in ST2 cells even in the presence of a PPAR-γ agonist. Supporting these *in vitro* observations, Wnt-5a$^{+/-}$ mice exhibited a reduction in bone mass presumably because of a reduced number of osteoblasts whereas increased numbers of adipocytes were seen in the bone marrow (Fig. 3b). Bone mass decrease was also detectable in Wnt-3a$^{+/-}$ mice (Fig. 3a, b, d, e) presumably owing to

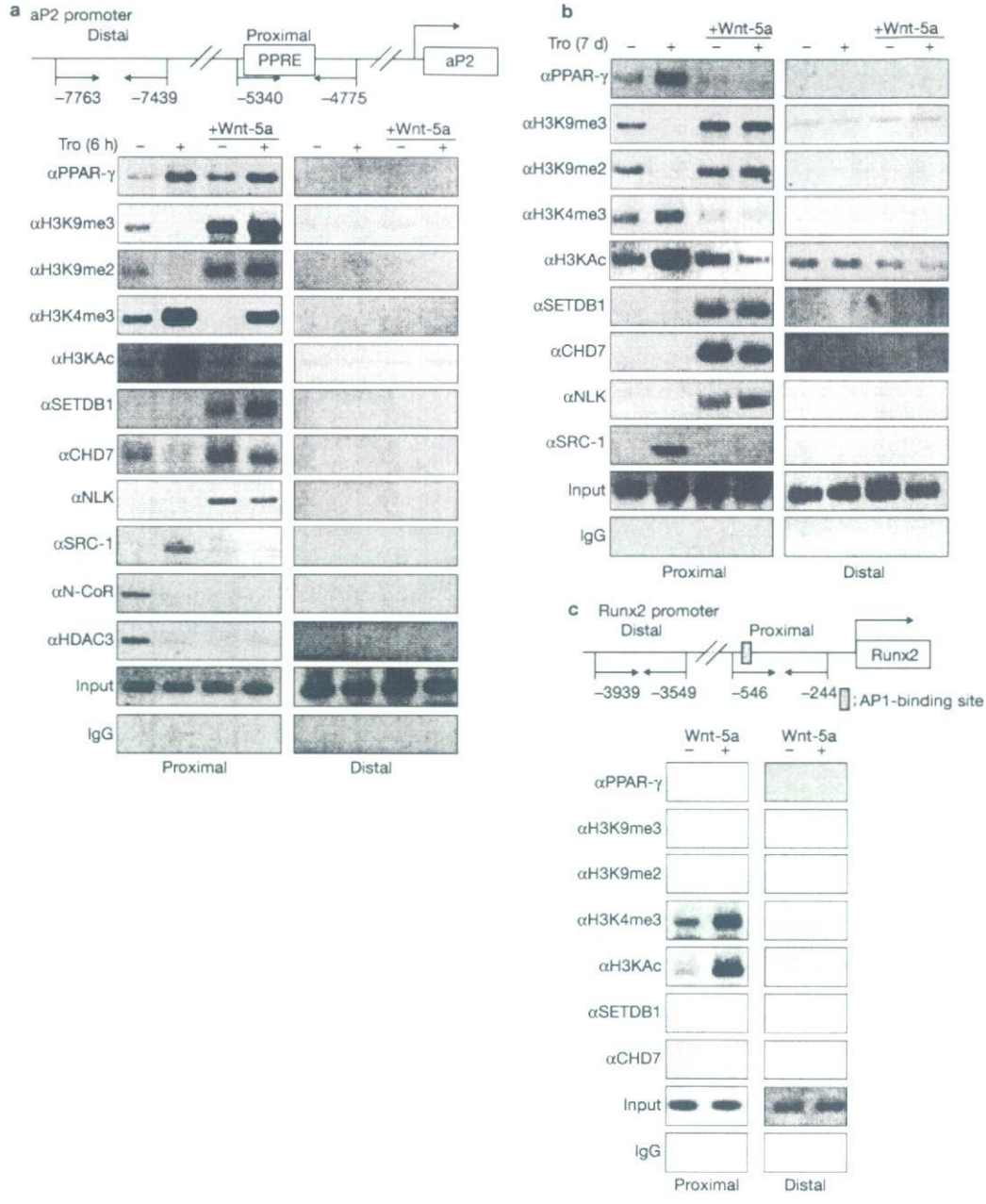

Figure 6 Wnt-5a-dependent recruitment of NLK containing corepressor complex. (**a**, **b**) Chromatin immunoprecipitation analysis of the aP2 promoter in ST2 cells treated with or without Troglitazone and Wnt-5a for 6 h (**a**) or 7days (**b**) was performed using indicated antibodies. (**c**) ChIP analysis of Runx2 promoter in ST2 cells. ST2 cells were treated with or without Wnt-5a, and ChIP analysis was performed using indicated antibodies.

impaired canonical Wnt signalling, consistent with recent reports that the canonical Wnt cascade through LRP5–β-catenin (LRP5: low-density lipoprotein receptor-related protein 5) is indispensable for osteoblastogenesis[33–35]. Wnt signalling thus seems to contribute to osteoblastogenesis from bone marrow mesenchymal cells through both canonical and non-canonical cascades. However, in terms of preventing the adipogenesis cell-lineage decision, only non-canonical Wnt signalling plays a significant part in bone marrow development.

It was recently reported that TAB2 in macrophage cells activated by the IL-1 signalling cascade prevents clearance of an HDAC co-repressor complex from ligand-bound sex steroid receptors, thus maintaining a transcriptionally repressive state of the steroid receptor[43]. In the present study, interestingly, an HDAC inhibitor (TSA) failed to abrogate the Wnt-5a effect on PPAR-γ transrepression (Fig. 4a), and, consistent with this finding, HDAC3 and N-CoR were not detected 6 h after Wnt-5a treatment (Fig. 6a). However, before Wnt-5a treatment in the absence of Tro, HDAC3 and N-CoR were associated with the promoter (Fig. 6a and Supplementary Information, Fig. S5a), and Wnt-5a seemed to induce clearance of the N-CoR-HDAC complex and block SRC-1 recruitment even in the presence of Tro. These findings clearly suggest that the

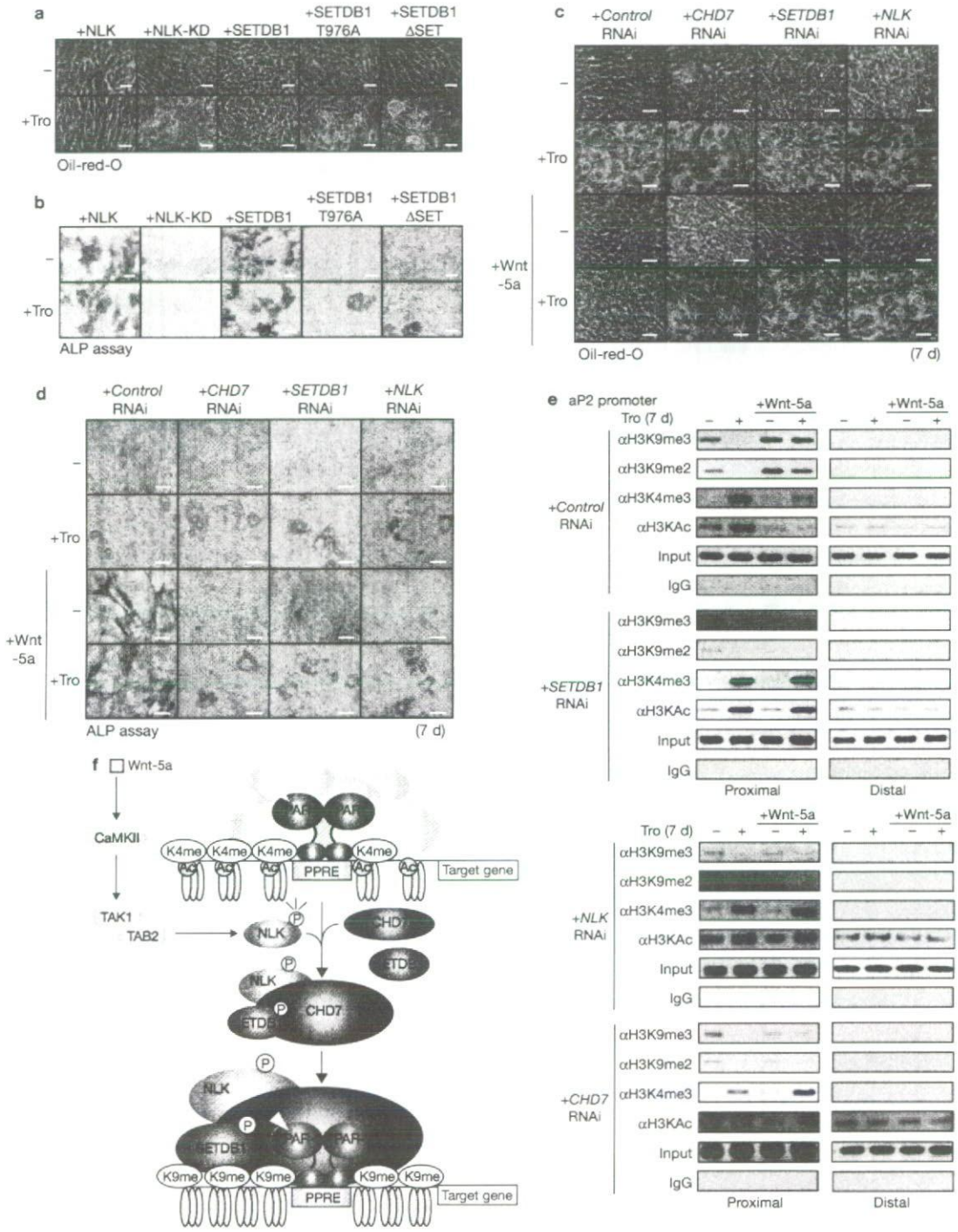

Figure 7 *NLK*, *SETDB1* and *CHD7* RNAi abrogated Wnt-5a-dependent differentiation and recruitment of modified H3. (**a**, **b**) ST2 cells overexpressed with NLK or SETDB1 mutants (NLK-KN, SETDB1T976A or SETDB1ΔSET) were incubated for 7 d, then stained with Oil-red-O (**a**) and ALP assay (**b**). Scale bars, 100 μm (**c**, **d**) *SETDB1* and *CHD7* RNAi abrogated the Wnt-5a dependent inhibition of adipogenesis. Control, *SETDB1* or *CHD7* RNAi adenovirus was infected in ST2 cells and stained with Oil-Red-O (**c**) or by ALP assay (**d**). (**e**) Chromatin immunoprecipitation analysis on aP2 promoter in ST2 cells expressing *SETDB1*, *NLK* or *CHD7* RNAi. (**f**) A mechanistic model for Wnt-5a dependent suppression of PPAR-γ function. Activated NLK through Wnt-5a-CaMKII–TAK1–TAB2 phosphorylates SETDB1. Then phosphorylated SETDB1 associates with CHD7 and act as a repressor for PPAR-γ transactivation function. CaMKII, calmodulin kinase II; PPRE, PPAR-response element; K4me, tri-methylated histone H3K4; K9me, tri-methylated histone H3K9; grey square, Wnt-5a.

transrepression of PPAR-γ by Wnt-5a mediates a histone-inactivating mechanism other than histone deacetylation by a HDAC co-repressor complex. We identified an HKMT, SETDB1, as an interacting partner of activated NLK by Wnt-5a by a biochemical approach. SETDB1 seems to form a complex with CHD7 and phosphorylated NLK. However, under our purification conditions, known SETDB1 partners such as human ATFa-associated modulator (hAM) were undetectable[23]. The SETDB1 complex associated with PPAR-γ to methylate H3-K9 in the PPAR-γ target gene promoters leading to inactivation of gene expression through histone-inactivating modifications. Thus, this complex is presumed to be a new type of HKMT co-repressor complex for nuclear receptors in terms of signalling dependency. These findings are supported by a recent report that several H3-K9 HKMTs serve as co-repressors for ligand-bound nuclear receptors[44,45], although signal-induced recruitment of HKMT to nuclear receptors was not reported. In this respect, it is notable in a previous report that repression of A-Myb by activated NLK through the Wnt-1–TAK1–TAB1–HIPK2 axis was mediated by an as yet unidentified HKMT[46]. SETDB1 might be a nuclear target activated by signalling of cell-membrane receptors to co-repress several classes of transcriptional factors.

SETDB1 is shown here to be integrated into a complex through phosphorylation by activated NLK, and it then serves as a co-repressor complex component with CHD7, a platform component. Interestingly, the HKMT activity of SETDB1 required complex formation induced by the non-canonical cascade. Given that hAM is reportedly a crucial partner for forming a complex with SETDB1 that has HKMT activity and can transcriptionally repress[23], SETDB1 might be a catalytic subunit that is fully functional only when integrated into distinct protein complexes. Co-activators and co-activator complexes are required for ligand-induced transactivation of PPAR-γ, but the SETDB1–NLK–CHD7 complex seems to attenuate recruitment of such co-activators to ligand-bound PPAR-γ. In this regard, CHD7 seems to be a docking component in the complex for PPAR-γ, considering the observed interaction of CHD7 with PPAR-γ *in vitro*. Moreover, because CHD7 harbours two chromodomains that selectively recognize and preferentially bind to methylated histone lysines[39], CHD7 could also anchor this complex to specific chromosomal regions. In fact, CHD7 was revealed to selectively interact with methylated H3-K4 and H3-K9, but not acetylated histones (Fig. 5g), implicating multiple roles of CHD7 in transcriptional repression. CHD7 may target the SETDB1 complex to transcriptionally active regions through interacting with methylated H3-K4, and then SETDB1 might initiate H3-K9 methylation in the PPAR-γ target gene promoters (Fig. 7f). At the present stage, it remains unclear whether methylated H3-K4 is an initial docking signal for recruiting the SETDB1 complex or whether this complex is first recruited to PPAR-γ. Furthermore, at later stages of the repression process, through stable retention of the SETDB1 complex through interaction of CHD7 with tri-methylated H3-K9 at the promoters, the SETDB1 complex might trigger heterochromatinization from transcriptionally silent euchromatin. In this respect, CHD7, but not SETDB1, might define the target specificity of the PPAR-γ target promoters by acting as an anchor to chromatin. Likewise, other silencing factors such as DNA methyltransferase and methyl-binding protein may be recruited through CHD7 to the target promoters for stable transrepression.

For every histone modification at a specific residue, multiple histone-modifying enzymes have been identified as recognizing the same histone residue. As recent findings have shown that histone-modifying enzymes often form complexes as enzymatically functional units[45], it is conceivable that complex components enable enzymes to specifically recognize histone residues as substrates and serve as regulatory subunits that integrate with intracellular signalling. Thus, the combination of histone-modifying enzymes with their complex partners might be prerequisite for their specific roles in gene regulation at the chromatin level. □

METHODS

Plasmid construction. Expression vectors of full-length PPAR-γ, PPAR-γ mutants (S8A, S112A and S8A-S112A), TAK1, TAK1^{K63W}, C/EBPβ, GR and acyl-CoA-PPRE-tk, GRE-tk, C/EBP-RE-tk luciferase reporter vectors, GST-fusion PPAR-γs (amino acids 1–506, 1–138, 139–311, 204–506) were constructed as previously described[15]. Expression vectors of CaMKII (WT, KN and TD) and Flag–NLK and Flag–NLK^{K155M} were constructed as previously described[20]. Deletion mutants of NLK (amino acids 1–443, 124–443, 124–517) and GFP-fusion mutants of NLK were amplified by polymerase chain reaction (PCR) and cloned into pcDNA3 (Invitrogen, Carlsbad, CA) and pGEX4T-1 (Amersham, Piscataway, NJ). SETDB1 and CHD7 were cloned by PCR and inserted into pcDNA3. SETDB1ΔSET(amino acid 1–660) was cloned by PCR and inserted into pcDNA3 and SETDB1 point mutants were generated by PCR-based mutagenesis using pcDNA3-SETDB1 as a template. For GST-fusion CHD7, CHD7 constructs (amino acids 231–364) were cloned by PCR and inserted into pGEX4T-1. The expression vector of Runx2 and Runx2-RE-tk luciferase reporter vector have been previously described[17]. For luciferase assays, the DNA sequence for RNAi against β-*catenin* and *NLK* were as follows: β-*catenin*, CACGCAAGAGCAA GTAGCTGATATT; *NLK*, GAAATATCTCCATTCAGCTGGCATT.

Cell culture, Wnt-5a treatment, transfection and luciferase assays. ST2 cells were cultured and examined using Oil-red-O staining and alkaline phosphatase assays as described previously[15]. For differentiation assays, cells were treated with or without 1 μM of Tro or 50 ng ml^{-1} of recombinant Wnt-5a (R&D Systems, Minneapolis, MN) for 7 d. GPDH activity was measured using the GPDH activity measurement kit (Takara, Ohtsu, Japan). The luciferase reporter assay was performed as previously described[15].

Animal preparation. The generation of Wnt-5a$^{+/-}$, Wnt-3a$^{+/-}$ and PPAR-γ$^{+/-}$ gene-target mice was previously described[32,36,47]. These mice were crossed with C57BL6 over five generations. All experiments were performed on male mice at 18 weeks of age, and mice littermates were fed a standard diet. All mice were maintained according to the protocol approved by the Animal Care and Use Committee of the University of Tokyo.

Analysis of skeletal morphology and μ-QCT imaging. The femora were collected from 18-week old WT, Wnt-5a$^{+/-}$, Wnt-3a$^{+/-}$ and PPAR-γ$^{+/-}$ mice and fixed in 70% ethanol. Femoral bone mineral densities were determined by dual-energy X-ray absorptiometry (DCS-600EX-III, ALOKA, Tokyo, Japan). Femur bone radiographs were obtained using a soft X-ray apparatus (TRS-1005, SOFTRON, Yokohama, Japan). Histomorphometric analysis for measurement of BV/TV, trabecular number and space was conducted by the Bone Analysis Service at Kureha Special Laboratory (Tokyo, Japan). For micro-quantitative computed tomography (μ-QCT) imaging, soft tissue was meticulously removed and placed in a special polycarbonate specimen tube filled with distilled water and scanned by ScanXmate-A100S40 (Comscan techno, Yokohama, Japan). Data sets with isotropic 8.6 μm voxel spacing were acquired at 0.45° steps over a total rotation of 360° at 80 kVp. Images were reconstructed into three-dimensional volumes using true Feldkamp reconstruction with 10-bit grey levels. To determine adipocytes in bone, an upper and lower pixel intensity threshold (LUT) was chosen (110–160; adipocytes). The highlighting tool was used to select individual adipose depots for pixel counting.

RNA analysis. Total cellular RNA was isolated from ST2 cells by ISOGEN (Wako, Tokyo, Japan), and quantitative reverse transcribed PCR (RT–PCR) was performed on a TP800 sequence detector (Takara, Ohtsu, Japan). The primers used are described in the Supplementary Information. For RT–PCR analysis, RT reaction was performed using SuperScript III (Invitrogen, Carlsbad, CA), and aggrecan (amino acids 150–290) and type II collagen (amino acids 1395–1451) were amplified by PCR.

Immunoprecipitation and ChIP analysis. The immunoprecipitation assay was performed as previously described[48]. For the ChIP assay, ST2 cells were incubated with or without Tro or Wnt-5a. We used the ChIP Assay Kit (Upstate, Lake Placid, NY) with antibodies against acetylated histone H3, trimethylK9H3 (Upstate), PPAR-γ, NLK (Santa Cruz Biotechnology, Santa Cruz, CA) or SETDB1 (Axxora, San Diego, CA). Antibody against CHD7 was produced by Asahi Technoglass (Funabashi, Japan). For PCR, we used the following primer pairs: 5′-AGTTC ACTAGTGGAAGTGTCACAGC-3′ (−5340 to −5315) and 5′-CTAGAAACAG ACACTGGAACCACTCT-3′ (−4800 to −4775) for aP2 gene promoter region at PPRE, and 5′-ACAGGCCTGCACAGAGGACGTTTCC-3′ (−7763 to −7739) and 5′-CATCATTTGCTATAAGTTGATTAGG-3′ (−7464 to −7439) for aP2 gene distal region. For amplification of Runx2 promoter by PCR, we used the primer pairs 5′-GGTAGAGAAGAGAGATGAAAAAGCAGAGG-3′ (−546 to −518) and 5′- GGTGTTCCTCTGTCTCTCCTTCCCT-3′ (−268 to −244) for the *Runx2* gene promoter region[49], and 5′-GCTACAATGTCGATATTCCTC-3′(−3939 to −3919) and 5′-GCATATCTGGTTGTGAGTAC-3′ (−3568 to −3549) for the *Runx2* gene distal region. Optimal PCR conditions for semi-quantitative measurement were 27 cycles of 30 s at 96 °C, 45 s at 56 °C, and 1 min at 72 °C. PCR products were visualized on 2% agarose-Tris-Acetate-EDTA (TAE) gels.

***In vitro* kinase assay and histone methylation assay.** For the *in vitro* phosphorylation assay, anti-Flag–NLK immunocomplexes were incubated with GST–SETDB1 (WT, T700A and T976A) in 10 μl of kinase buffer containing 10 mM HEPES (pH 7.4), 1 mM dithiothreitol (DTT), 5 mM $MgCl_2$ and 5 μCi of [γ^{32}P]ATP at 25 °C for 10 min. Samples were resolved by SDS polyacrylamide gel electrophoresis (SDS-PAGE), and phosphorylated proteins were visualized by imaging analyser BAS1500 (Fujifilm, Tokyo, Japan). For the histone methyltransferase assay, we used aliquots of anti-Flag–NLK immunocomplexes and the HMT assay kit (Upstate).

Protein purification. For NLK–PPAR-γ complex purification, HeLa cells stably expressing Flag–NLK were incubated with 50 mM KCl for 30 min, and nuclear extracts were prepared as previously described[37,38]. Then extracts were bound to the GST–PPAR-γ column, and complexes bound to PPAR-γ were eluted with 15 mM reduced glutathione in elution buffer (50 mM Tris-HCl, pH 8.3, 150 mM KCl, 0.5 mM EDTA, 0.5 mM PMSF, 5 mM CHD7, 0.08% NP-40 and 10% glycerol) and loaded onto an anti-Flag M2 resin column (Sigma, St Louis, MO), washed with binding buffer, and eluted by incubation for 60 min with 0.5 ml of the Flag peptide (0.2 mg ml^{-1}) (Sigma) in binding buffer. After elution, proteins were identified by MALDI-TOF mass spectroscopy (Voyager, Applied Biosystems, Foster City, CA). For glycerol density gradient fractionation, they were layered on top of a 4.5 ml linear 100%–40% glycerol gradient in the binding buffer and centrifuged for 16 h at 4 °C at 40,000 r.p.m. in a SW40 rotor (Beckman Coulter, Fullerton, CA).

Pull-down assays. NLK (amino acids 1–443, 124–517), SETDB1 (amino acids 661–1291), PPAR-γ mutants (amino acids 1–138, 139–311, 204–506, 1–506) were expressed as a GST fusion protein in *Escherichia coli* strain HB101. The expression of a protein of the predicted size was then monitored by SDS-PAGE. GST pull-down assays using [^{35}S]-methionine-labelled CHD7, CHD7$^{1-1107}$, NLK and SETDB1 were performed as previously described[15]. Peptide pull-down assays using GST–CHD7 (amino acids 231–364) were performed as previously described[50]. For histone-binding assays, GST proteins were incubated with semi-purified HeLa histones in 300 mM NaCl, 50 mM Tris-HCl (pH 7.5), 5 mM EDTA (pH 7.9), 0.5% NP40 for 2 h at room temperature. After washing three times in 500 mM NaCl, 50 mM Tris-HCl (pH 7.5), 5 mM EDTA (pH 7.9), 0.5% NP40, samples were separated by SDS-PAGE and western blotting was performed.

Adenoviral constructs and transduction. The adenoviral vector expressing RNAi against murine *NLK*, murine *SETDB1*, and murine *CHD7* were constructed from pSIREN and Adeno-X (Clontech, Palo Alto, CA). The RNAi oligonucleotide sequences are as follows: Control, CTGGACTTCCAGAAGAAATT; *NLK*, GCAGCCGTCATTACAGCAA; *SETDB1*, GGTGATGAGTACTTTGCAA; *CHD7*, GCAATCATCCCTACCTAAT. Adeno-X plasmids were digested with *PacI* and cotransfected into 293T cells using Lipofectamine Plus (Invitrogen, Carlsbad, CA). Virus-containing supernatants were collected at 48 h post-transfection and passed through a 0.45 μm filter.

Note: Supplementary Information is available on the Nature Cell Biology website.

ACKNOWLEDGEMENTS

We thank A. P. Kouzmenko, M. Kim and R. Fujiki for helpful discussions and H. Higuchi and S. Fujiyama for manuscript preparation. And we also thank S. Ishii (RIKEN Tsukuba Institute) for helpful advice and T. Komori (Nagasaki University) for the kind gift of the *Runx2* expression vector and reporter vector. This work was supported, in part, by a Grant-In-Aid for Basic Research Activities for Innovative Biosciences (BRAIN) and Priority Areas from the Ministry of Education, Science, Sports, and Culture of Japan (to S.K.).

Published online at http://www.nature.com/naturecellbiology/
Reprints and permissions information is available online at http://npg.nature.com/reprintsandpermissions

1. Fischle, W., Wang, Y. & Allis, C. D. Histone and chromatin cross-talk. *Curr. Opin. Cell Biol.* **15**, 172–183 (2003).
2. Margueron, R., Trojer, P. & Reinberg, D. The key to development: interpreting the histone code? *Curr. Opin. Genet. Dev.* **15**, 163–176 (2005).
3. Martin, C. & Zhang, Y. The diverse functions of histone lysine methylation. *Nature Rev. Mol. Cell Biol.* **6**, 838–849 (2005).
4. Bannister, A. J. & Kouzarides, T. Reversing histone methylation. *Nature* **436**, 1103–1106 (2005).
5. Metzger, E., Wissmann, M. & Schule, R. Histone demethylation and androgen-dependent transcription. *Curr. Opin. Genet. Dev.* **16**, 513–517 (2006).
6. Wu, R. C., Smith, C. L. & O'Malley, B. W. Transcriptional regulation by steroid receptor coactivator phosphorylation. *Endocr. Rev.* **26**, 393–399 (2005).
7. Dilworth, F. J. & Chambon, P. Nuclear receptors coordinate the activities of chromatin remodeling complexes and coactivators to facilitate initiation of transcription. *Oncogene* **20**, 3047–3054 (2001).
8. Rosenfeld, M. G., Lunyak, V. V. & Glass, C. K. Sensors and signals: a coactivator/corepressor/epigenetic code for integrating signal-dependent programs of transcriptional response. *Genes Dev.* **20**, 1405–1428 (2006).
9. Pascual, G. *et al.* A SUMOylation-dependent pathway mediates transrepression of inflammatory response genes by PPAR-gamma. *Nature* **437**, 759–763 (2005).
10. Evans, R. M., Barish, G. D. & Wang, Y. X. PPARs and the complex journey to obesity. *Nature Med.* **10**, 355–361 (2004).
11. Feige, J. N., Gelman, L., Michalik, L., Desvergne, B. & Wahli, W. From molecular action to physiological outputs: peroxisome proliferator-activated receptors are nuclear receptors at the crossroads of key cellular functions. *Prog. Lipid Res.* **45**, 120–159 (2006).
12. Lehrke, M. & Lazar, M. A. The many faces of PPARgamma. *Cell* **123**, 993–999 (2005).
13. Tontonoz, P., Hu, E., Graves, R. A., Budavari, A. I. & Spiegelman, B. M. mPPAR gamma 2: tissue-specific regulator of an adipocyte enhancer. *Genes Dev.* **8**, 1224–1234 (1994).
14. Hu, E., Kim, J. B., Sarraf, P. & Spiegelman, B. M. Inhibition of adipogenesis through MAP kinase-mediated phosphorylation of PPARgamma. *Science* **274**, 2100–2103 (1996).
15. Suzawa, M. *et al.* Cytokines suppress adipogenesis and PPAR-gamma function through the TAK1/TAB1/NIK cascade. *Nature Cell Biol.* **5**, 224–230 (2003).
16. Chien, K. R. & Karsenty, G. Longevity and lineages: toward the integrative biology of degenerative diseases in heart, muscle, and bone. *Cell* **120**, 533–544 (2005).
17. Harada, S. & Rodan, G. A. Control of osteoblast function and regulation of bone mass. *Nature* **423**, 349–355 (2003).
18. Ralston, S. H. & de Crombrugghe, B. Genetic regulation of bone mass and susceptibility to osteoporosis. *Genes Dev.* **20**, 2492–2506 (2006).
19. Behrens, J. *et al.* Functional interaction of beta-catenin with the transcription factor LEF-1. *Nature* **382**, 638–642 (1996).
20. Ishitani, T. *et al.* The TAK1-NLK mitogen-activated protein kinase cascade functions in the Wnt-5a/Ca(2+) pathway to antagonize Wnt/beta-catenin signaling. *Mol. Cell. Biol.* **23**, 131–139 (2003).
21. Veeman, M. T., Axelrod, J. D. & Moon, R. T. A second canon. Functions and mechanisms of beta-catenin-independent Wnt signaling. *Dev. Cell* **5**, 367–377 (2003).
22. Schultz, D. C., Ayyanathan, K., Negorev, D., Maul, G. G. & Rauscher, F. J. 3rd. SETDB1: a novel KAP-1-associated histone H3, lysine 9-specific methyltransferase that contributes to HP1-mediated silencing of euchromatic genes by KRAB zinc-finger proteins. *Genes Dev.* **16**, 919–932 (2002).
23. Wang, H. *et al.* mAM facilitates conversion by ESET of dimethyl to trimethyl lysine 9 of histone H3 to cause transcriptional repression. *Mol. Cell* **12**, 475–487 (2003).
24. Vissers, L. E. *et al.* Mutations in a new member of the chromodomain gene family cause CHARGE syndrome. *Nature Genet.* **36**, 955–957 (2004).
25. Komatsu, Y. *et al.* Targeted disruption of the Tab1 gene causes embryonic lethality and defects in cardiovascular and lung morphogenesis. *Mech. Dev.* **119**, 239–249 (2002).
26. Ishitani, T. *et al.* The TAK1-NLK-MAPK-related pathway antagonizes signalling between beta-catenin and transcription factor TCF. *Nature* **399**, 798–802 (1999).
27. Almind, K. & Kahn, C. R. Genetic determinants of energy expenditure and insulin resistance in diet-induced obesity in mice. *Diabetes* **53**, 3274–3285 (2004).
28. Mueller, E. *et al.* Terminal differentiation of human breast cancer through PPAR gamma. *Mol. Cell* **1**, 465–470 (1998).

29. Hong, J. H. *et al.* TAZ, a transcriptional modulator of mesenchymal stem cell differentiation. Science **309,** 1074–1078 (2005).
30. Schwartz, A. V. *et al.* Thiazolidinedione use and bone loss in older diabetic adults. *J. Clin. Endocrinol. Metab.* **91,** 3349–3354 (2006).
31. Akune, T. *et al.* PPARgamma insufficiency enhances osteogenesis through osteoblast formation from bone marrow progenitors. *J. Clin. Invest.* **113,** 846–855 (2004).
32. Takada, S. *et al.* Wnt-3a regulates somite and tailbud formation in the mouse embryo. *Genes Dev.* **8,** 174–189 (1994).
33. Glass, D. A. 2nd *et al.* Canonical Wnt signaling in differentiated osteoblasts controls osteoclast differentiation. *Dev. Cell* **8,** 751–764 (2005).
34. Gong, Y. *et al.* LDL receptor-related protein 5 (LRP5) affects bone accrual and eye development. *Cell* **107,** 513–523 (2001).
35. Ross, S. E. *et al.* Inhibition of adipogenesis by Wnt signaling. *Science* **289,** 950–953 (2000).
36. Yamaguchi, T. P., Bradley, A., McMahon, A. P. & Jones, S. A Wnt5a pathway underlies outgrowth of multiple structures in the vertebrate embryo. *Development* **126,** 1211–1223 (1999).
37. Kitagawa, H. *et al.* The chromatin-remodeling complex WINAC targets a nuclear receptor to promoters and is impaired in Williams syndrome. *Cell* **113,** 905–917 (2003).
38. Yanagisawa, J. *et al.* Nuclear receptor function requires a TFTC-type histone acetyl transferase complex. *Mol. Cell* **9,** 553–562 (2002).
39. Brehm, A., Tufteland, K. R., Aasland, R. & Becker, P. B. The many colours of chromodomains. *Bioessays* **26,** 133–140 (2004).
40. Botrugno, O. A. *et al.* Synergy between LRH-1 and beta-catenin induces G1 cyclin-mediated cell proliferation. *Mol. Cell* **15,** 499–509 (2004).
41. Kouzmenko, A. P. *et al.* Wnt/beta-catenin and estrogen signaling converge *in vivo*. *J. Biol. Chem.* **279,** 40255–40258 (2004).
42. Asahina, M., Valenta, T., Silhankova, M., Korinek, V. & Jindra, M. Crosstalk between a nuclear receptor and beta-catenin signaling decides cell fates in the *C. elegans* somatic gonad. *Dev. Cell* **11,** 203–211 (2006).
43. Zhu, P. *et al.* Macrophage/cancer cell interactions mediate hormone resistance by a nuclear receptor derepression pathway. *Cell* **124,** 615–629 (2006).
44. Garcia-Bassets, I. *et al.* Histone methylation-dependent mechanisms impose ligand dependency for gene activation by nuclear receptors. *Cell* **128,** 505–518 (2007).
45. Wang, J. *et al.* Opposing LSD1 complexes function in developmental gene activation and repression programmes. *Nature* **446,** 882–887 (2007).
46. Kurahashi, T., Nomura, T., Kanei-Ishii, C., Shinkai, Y. & Ishii, S. The Wnt-NLK signaling pathway inhibits A-Myb activity by inhibiting the association with coactivator CBP and methylating histone H3. *Mol. Biol. Cell* **16,** 4705–4713 (2005).
47. Kubota, N. *et al.* PPAR gamma mediates high-fat diet-induced adipocyte hypertrophy and insulin resistance. *Mol. Cell* **4,** 597–609 (1999).
48. Ohtake, F. *et al.* Modulation of oestrogen receptor signalling by association with the activated dioxin receptor. *Nature* **423,** 545–550 (2003).
49. Fujiwara, M. *et al.* Isolation and characterization of the distal promoter region of mouse Cbfa1. *Biochim. Biophys. Acta* **1446,** 265–272 (1999).
50. Fujiki, R. *et al.* Ligand-induced transrepression by VDR through association of WSTF with acetylated histones. *EMBO J.* **24,** 3881–3894 (2005).

nature
cell biology

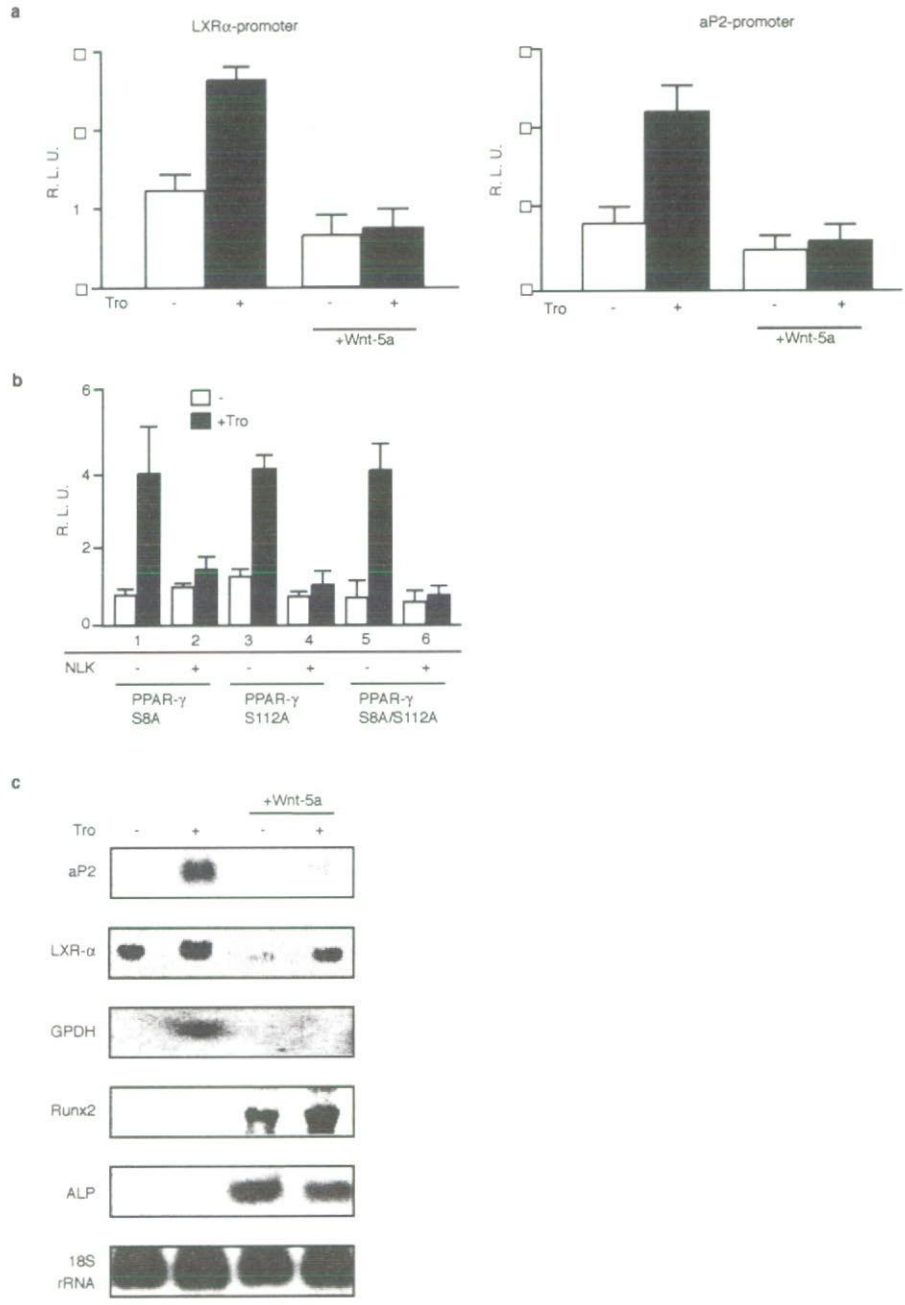

Figure S1. Supplemental data on luciferase reporter assays. (**a**) Luciferase assay in ST2 cells. After transfection with expression vectors of PPAR-γ and each reporter vectors ST2 cells were cultured with or without Wnt-5a for 24hrs and luciferase assay was performed. (**b**) Lusiferase assay in ST2 cells transfected with expression vectors of MAPK phosphorylation mutants of PPAR-γ (S8A, S112A, S8A-S112A), NLK and PPRE-tk-luc vectors. In (**a**) and (**b**), error bars represent the means +/- S. D. of triplicate, independent determinations. **(c)** Northern blot analysis for differentiation markers of adipocytes (aP2, GPDH and LXR-α) and osteoblasts (ALP and Runx2) in ST2 cells incubated with or without Wnt-5a and Tro were performed.

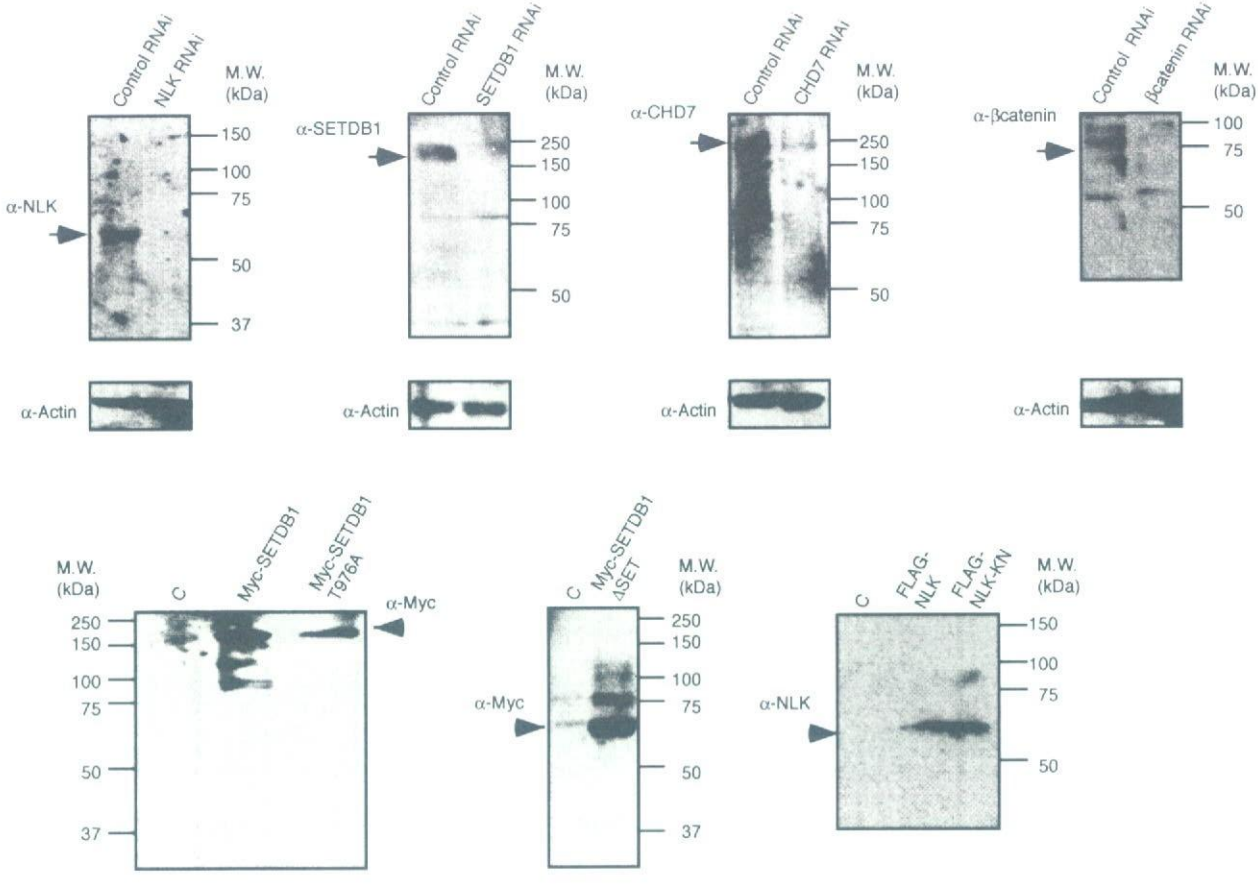

Figure S2. Supplemental data on protein expression. Each nuclear-cell extracts were prepared and then western blotting was performed.

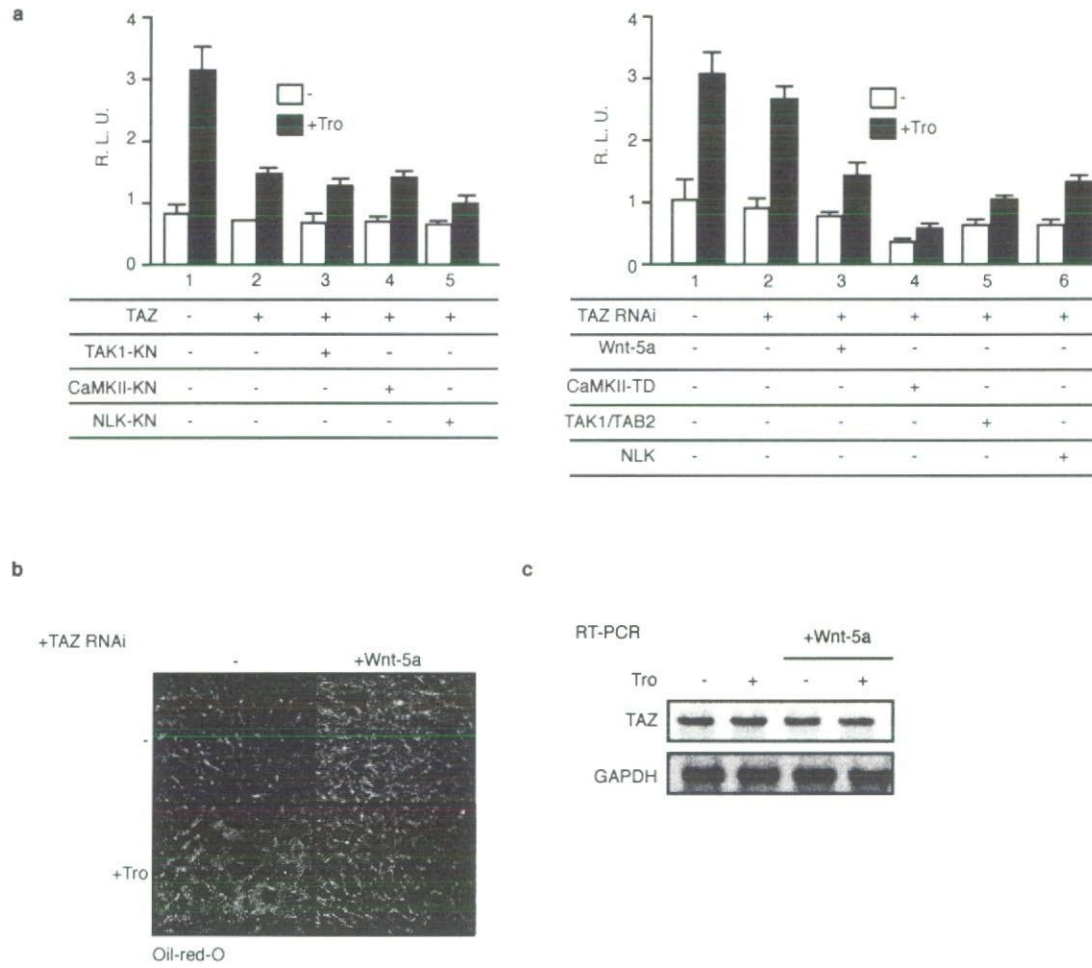

Figure S3. Supplemental data on TAZ function in Wnt-5a signaling. (**a**) Luciferase assay transfected with PPRE-tk-luc vector and indicated vectors were performed. Error bars represent the means +/- S. D. of triplicate, independent determinations. (**b**) TAZ RNAi did not abrogate Wnt-5a induced inhibition of adipogenesis. ST2 cells were transfected with adenovirus expressing mTAZ-specific RNAi and were then transferred to adipocyte differentiation medium. Cells were stained by Oil-red O. Scale bars, 100 μm. (**c**) Expression level of TAZ mRNA was not changed when treated with or without Tro or Wnt-5a in (**b**). RT-PCR was performed.

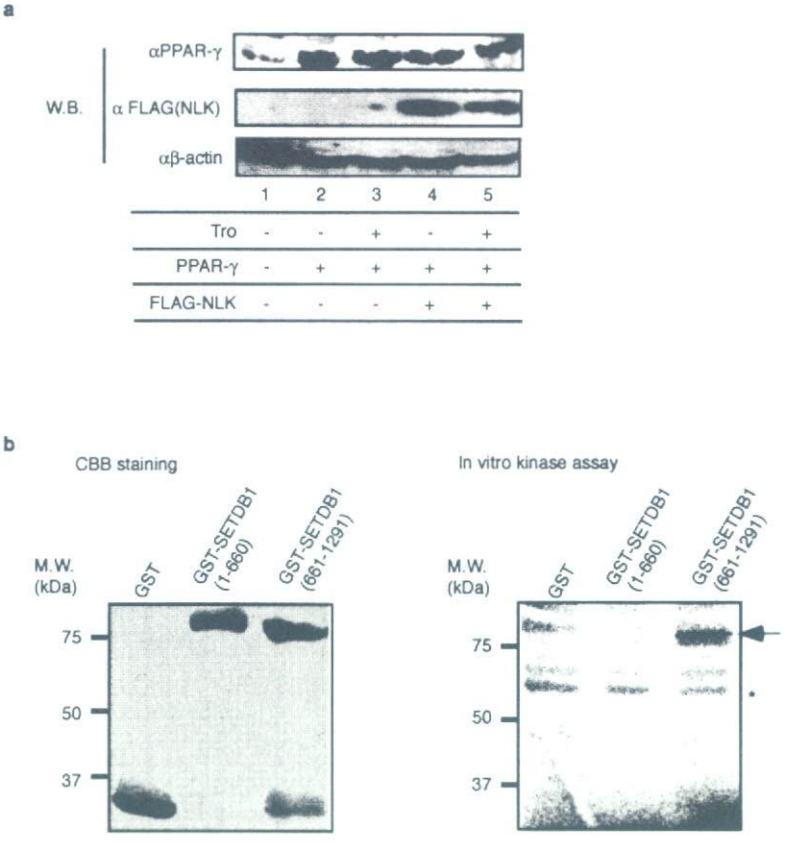

Figure S4. (a) Supplemental data on the degradation of PPAR-γ by NLK. ST2 cells were transfected with NLK expression vector and then lysates were performed for western blotting with antibody against PPAR-γ. **(b)** In vitro kinase assay using GST, GST-SETDB1 (1-660 amino aicds), and GST-SETDB1 (661-1291 amino acids). GST fused proteins were incubated with anti-FLAG-NLK immunocomplexes and [^{32}P]γ-ATP. Arrow head indicates phosphorylated GST-SETDB1 (661-1291 amino acids) and asterisk indicates self-phosphoerylated NLK.

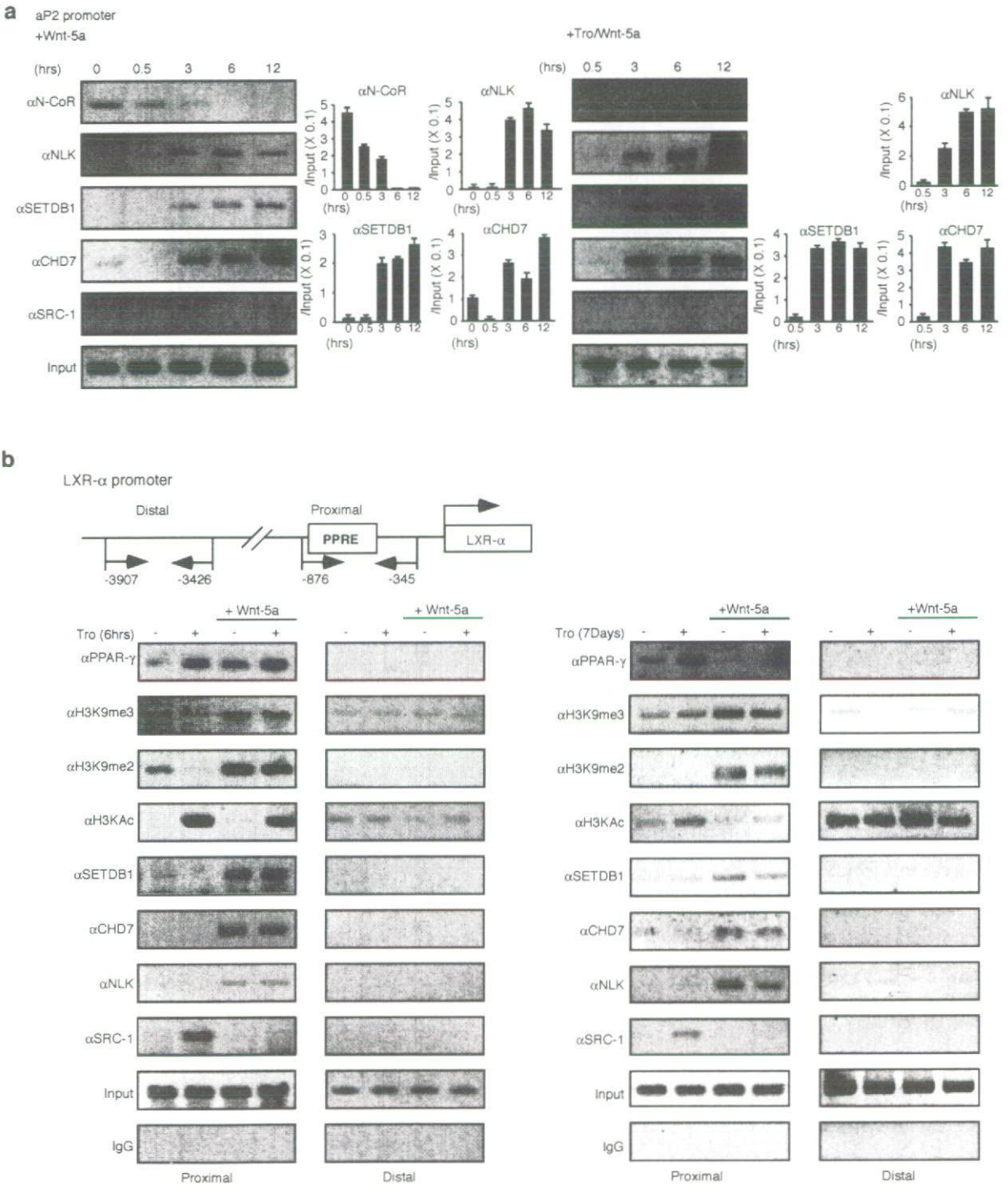

Figure S5. Supplemental data on the ChIP analysis. (**a**) Time-coursed ChIP analysis on aP2 promoter in ST2 cells. After treated with or without Tro or Wnt-5a, each time-coursed ChIP analysis was performed by using indicated antibodies. Recruitment intensity was shown as each graph. Error bars represent the means +/- S. D. of triplicate, independent determinations. (**b**) ChIP analysis on LXR-α promoter in ST2 cells. ST2 cells were treated with/without Tro and Wnt-5a for 6 hrs (left panel) or 7days (right panel). Then ChIP analysis was performed with indicated antibodies on LXR-α promoter region.

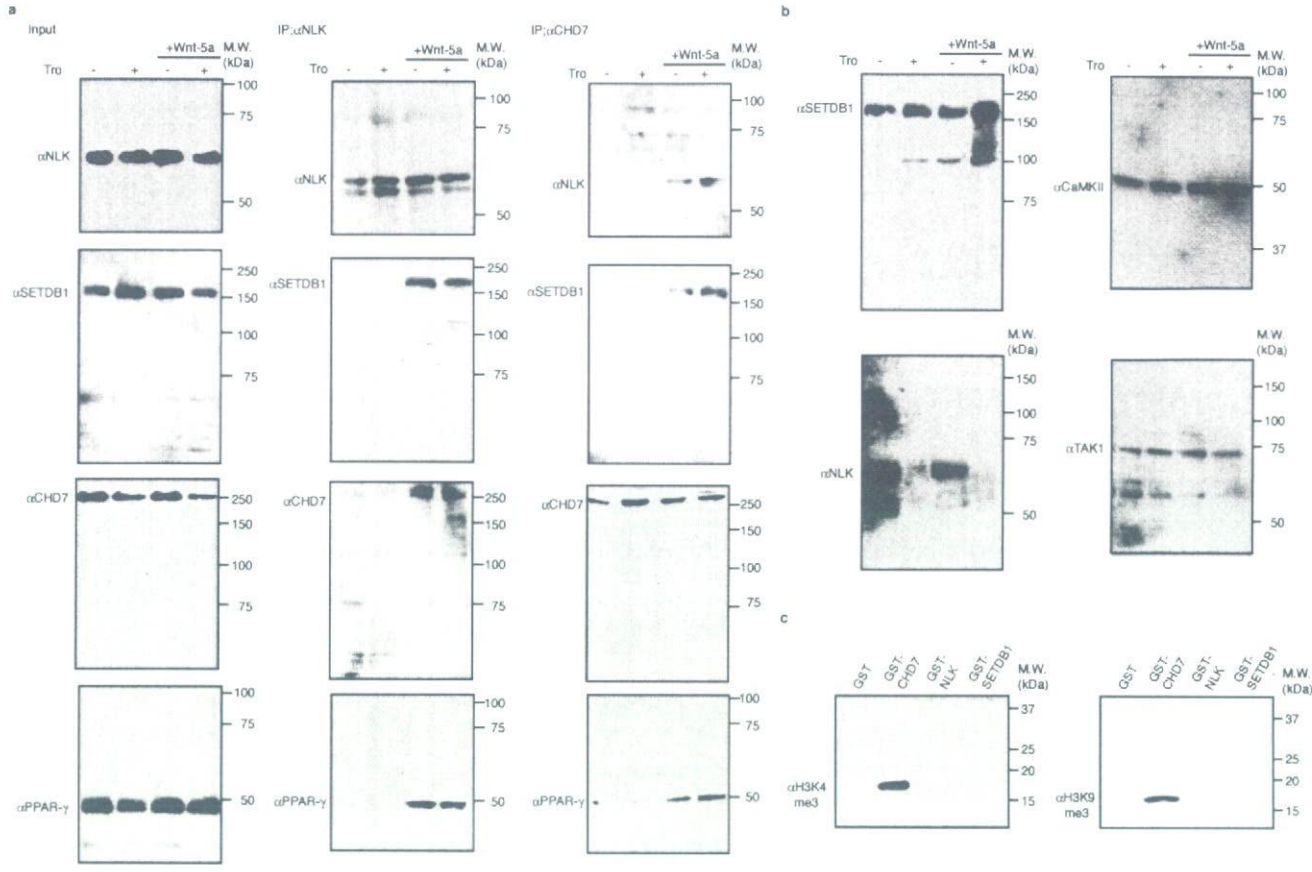

Figure S6. Selected representative full-scan images. Full sized membranes were cut prior to immunoblotting according to prestained MW markers. **(a)** Images correspond to Fig. 4e. **(b)** Images correspond to Fig. 5a left panel. **(c)** Images correspond to Fig. 5g.

Reference

1. Hong, J. H. et al. TAZ, a transcriptional modulator of mesenchymal stem cell differentiation. Science 309, 1074-8 (2005).

Supplementary Information

MATERIALS

The primers used for quantitative RT-PCR were as follows;

aP2; 5'-TGGGAACCTGGAAGCTTGTCTC-3' for forward primer and 5'-GCTGATGATCATGTTGGGCTTG-3' for reverse primer.

ALP; 5'-ACACCTTGACTGTGGTTCTGCTGA-3' for forward primer and 5'-CCTTGTAGCCAGGCCCGTTA-3' for reverse primer.

Runx2; 5'-CATTTGCACTGGGTCACACGTA-3' for forward primer and 5'-GAATCTGGCCATGTTTGTGCTC-3' for reverse primer.

LXR-α; 5'-TGCAGGACCAGCTCCAAGTAGA-3' for forward primer and 5'-GGCTCACCAGCTTCATTAGCATC-3' for reverse primer.

GPDH; 5'-GGGCTGAAGCTAATCTCCGACA-3' for forward primer and 5'-AGGCCGTTCTGCTCACTTTG-3' for reverse primer.

ChIP analysis was performed as described in the text. Used primers for ChIP analysis were 5'-AGTTCAGCACAGAAGTGCTTTCCTAGC-3' (-876 to -850) and 5'-CCCATCTGAGATGGTGTCAAGATCTAC-3' (-372 to -345) for the LXR-α gene promoter region at PPRE, and 5'-CGCCCGGATGCATTCGTAAGGA-3' (-3907 to -3886) and 5'-GGCTGGTTACATGCAGTACCCT-3' (-3447 to -3426) for LXR-α gene distal region.

Reporter vectors of aP2 promoter (-4246 to -6025)-tk-luc or LXR-α promoter (-1 to

-1650)-tk-luc were cloned by PCR and inserted into pGL3-tk-luc. Mouse TAZ1 cDNA was cloned by PCR and inserted into pcDNA3. RNAi sequence of TAZ1 was same as previously described[1]. Primers for RT-PCR were as follows; Fw; 5'-AATCCGTCCTCGGTGCCCCATCCGC-3', Rev; 5'-TTACAGCCAGGTTAGAAAGG-3'.

MOLECULAR AND CELLULAR BIOLOGY, July 2007, p. 4807–4814 Vol. 27, No. 13
0270-7306/07/$08.00+0 doi:10.1128/MCB.02039-06

The Pituitary Function of Androgen Receptor Constitutes a Glucocorticoid Production Circuit▽

Junko Miyamoto,[1]† Takahiro Matsumoto,[1,2]† Hiroko Shiina,[1] Kazuki Inoue,[1] Ichiro Takada,[1] Saya Ito,[1] Johbu Itoh,[3] Takeo Minematsu,[4] Takashi Sato,[1] Toshihiko Yanase,[5] Hajime Nawata,[5] Yoshiyuki R. Osamura,[4] and Shigeaki Kato[1,2]*

Institute of Molecular and Cellular Biosciences, University of Tokyo, 1-1-1 Yayoi, Bunkyo-ku, Tokyo 113-0032, Japan[1]; ERATO, Japan Science and Technology Agency, 4-1-8 Honcho, Kawaguchisi, Saitama 332-0012, Japan[2]; Teaching and Research Support Center[3] and Department of Pathology,[4] Tokai University School of Medicine, Boseidai, Isehara, Kanagawa 259-1193, Japan; and Department of Medicine and Bioregulatory Science, Graduate School of Medical Sciences, Kyushu University, Fukuoka 812-8582, Japan[5]

Received 1 November 2006/Returned for modification 18 December 2006/Accepted 16 April 2007

Androgen receptor (AR) mediates diverse androgen actions, particularly reproductive processes in males and females. AR-mediated androgen signaling is considered to also control metabolic processes; however, the molecular basis remains elusive. In the present study, we explored the molecular mechanism of late-onset obesity in male AR null mutant (ARKO) mice. We determined that the obesity was caused by a hypercorticoid state. The negative feedback system regulating glucocorticoid production was impaired in ARKO mice. Male and female ARKO mice exhibited hypertrophic adrenal glands and glucocorticoid overproduction, presumably due to high levels of adrenal corticotropic hormone. The pituitary glands of the ARKO males had increased expression of proopiomelanocortin and decreased expression of the glucocorticoid receptor (GR). There were no overt structural abnormalities and no alteration in the distribution of cell types in the pituitaries of male ARKO mice. Additionally, there was normal production of the other hormones within the glucocorticoid feedback system in both the pituitary and hypothalamus. In a cell line derived from pituitary glands, GR expression was under the positive control of the activated AR. Thus, this study suggests that the activated AR supports the negative feedback regulation of glucocorticoid production via up-regulation of GR expression in the pituitary gland.

Sex steroid hormones exert a wide variety of biological actions. They are also involved in pathological events, such as the development of hormone-dependent cancers in reproductive organs (5, 37). In vertebrates, sex hormones play a pivotal role in male reproductive function and metabolic control. Most sex steroid actions are mediated through transcriptional control of target genes by nuclear receptors (NRs). NRs form a gene superfamily and act as transcriptional factors (9, 20). Sex hormone receptors have been shown to transactivate particular sets of target genes in a hormone-dependent manner through direct DNA binding to specific elements in target gene promoters. Hormone receptors activated by hormone binding recruit a number of coregulator-coregulator complexes for transactivation (28). These complexes then affect transcription through chromatin remodeling (12, 17, 22) and histone modification (1, 7). Hormone binding to the receptors may also transrepress target genes. The mechanisms of hormone-dependent transrepression of steroid receptors likely involve protein-protein interactions and are thus more diverse than that of transactivation (8, 10, 13, 21).

The molecular mechanisms behind the regulation of gene transcription by hormones and their NRs are complicated. Gene disruption studies have clarified the role of various NRs in steroid hormone action. By combining a Cre-loxP system with a canonical gene disruption approach, we succeeded in disrupting the androgen receptor (AR) on the X chromosome in mice in a manner that did not result in male infertility (14). Male AR null mutant (ARKO) mice exhibit abnormalities typical of testicular feminization mutants, including female external genitalia with atrophic testis and impaired sex behavior (29). Growth of the male ARKO mice is partially retarded, with impaired bone growth coupled with high bone turnover (16). The male mice also develop late-onset obesity (30). In contrast, no clear phenotypic abnormalities are present in female ARKO mice. However, normal folliculogenesis does require the AR, which suggests that androgen/AR signaling is also physiologically important in females (32).

To study how and why obesity develops in ARKO males, we began by examining the adrenal glands, which were hypertrophic in both males and females. In the present study, we explored the molecular basis of this observation. Dissection of the gland revealed that the layers of the zona fasciculata were thicker and coupled to the remaining layers of the X-zone (fetal zone). The hypertrophy resulted from a hypercorticoid state. Adrenal corticotropic hormone (ACTH) overproduction was driven by impaired negative feedback through the hypothalamus-pituitary-adrenal (HPA) axis. No clear alteration in the numbers of hormone-producing cells in the pituitary glands and hypothalamus was detected, but there were increased proopiomelanocortin (POMC) and decreased glucocorticoid

* Corresponding author. Mailing address: Institute of Molecular and Cellular Biosciences, University of Tokyo, 1-1-1 Yayoi, Bunkyo-ku, Tokyo 113-0032, Japan. Phone: 81-8-5841-8478. Fax: 81-3-5841-8477. E-mail: uskato@mail.ecc.u-tokyo.ac.jp.

† J.M. and T.M. contributed equally to this work.

▽ Published ahead of print on 30 April 2007.

receptor (GR) expression levels of transcripts in the ARKO pituitary glands. Androgen-induced GR gene activation was further confirmed in a pituitary gland-derived cell line (AtT-20 cells). These findings suggest that androgen/AR signaling in the pituitary gland supports the normal feedback system of glucocorticoid production through the HPA axis.

MATERIALS AND METHODS

Animals. ARKO mice were generated by targeted disruption of the AR gene by means of a Cre-loxP system (19) and maintained as described previously (16, 29, 30, 32). Experiments were performed with 2- to 25-week-old male mice. All mice protocols were approved by the Animal Care and Use Committee of the University of Tokyo (31, 40).

Cell culture. Adherent AtT-20 cells, a murine corticotropic tumor cell line, were cultured in a 5% CO_2 atmosphere at 37°C with Dulbecco's modified Eagle's medium-Ham's F12 at 1:1 containing 15% fetal calf serum (FCS) and penicillin-streptomycin. 3T3-L1 cells, a murine preadipocyte cell line, were cultured with Dulbecco's modified Eagle's medium containing 10% FCS. FCS in the culture media was replaced with charcoal-treated FCS for 1 week prior to the administration of 5α-dihydrotestosterone (DHT). For Northern and Western blot analyses, the cultured AtT-20 cells were subcultured in six-well plates. After incubation for 24 h, DHT (10^{-7} M) was added to the medium.

Histology and immunohistochemistry. Adrenal glands and pituitary glands were fixed by immersion with 4% paraformaldehyde for 24 h at 4°C. They were then embedded in paraffin, sliced into 4-μm sections by standard methods, and mounted onto silane-coated slides. After perfusion by 0.9% saline followed by 4% paraformaldehyde, brains were postfixed in the same fixative for 2 h at 4°C and soaked in phosphate-buffered saline containing 20% sucrose. Frontal sections were cut at 30-μm thickness using a cryostat. Serial sections were divided into four groups and used for single-labeling immunohistochemistry for the GR, corticotropin-releasing hormone (CRH), α-melanocyte-stimulating hormone (α-MSH), or thionin to allow determination of the areas to be measured.

Immunostaining was carried out using antibodies as described below (34). The primary antibodies included rabbit polyclonal anti-human AR (N-20; Santa Cruz Biotechnology, Santa Cruz, CA), rabbit polyclonal anti-GR (M-20; Santa Cruz Biotechnology, Santa Cruz, CA), mouse anti-human ACTH (DAKO, Carpinteria, CA), mouse anti-human luteinizing hormone β (Immunotech, Marseille, France), mouse anti-human follicle-stimulating hormone β (DAKO, Carpinteria, CA), mouse anti-human thyroid-stimulating hormone β (Advanced Immunochemical Inc., CA), rabbit anti-rat glycoprotein hormone (kindly supplied by A. F. Parlow, the National Institute of Diabetes and Digestive and Kidney Diseases [NIDDK], Bethesda, MD), rabbit anti-human growth hormone (DAKO, Carpinteria, CA), and rabbit anti-rat prolactin (kindly supplied by A. F. Parlow, NIDDK).

After treatment with 0.5% H_2O_2 (30 min) and 5% normal serum (1 h), the sections were incubated for 24 h at 4°C with specific primary antibodies. The sections were then incubated with secondary antibodies and an avidin-biotin complex (Vectastain ABC Elite kit; Vector Laboratories). The signals were visualized with diaminobenzidine and the nuclei were counterstained with hematoxylin.

For dual labeling of ACTH and the AR or GR, a single staining of the AR or GR was first performed as described above. After the primary antibodies were removed by treatment with 0.1 M glycine, sections were incubated with anti-ACTH antibodies followed by alkaline phosphatase-conjugated anti-mouse immunoglobulin G (DAKO, Carpinteria, CA). The signals were visualized with 5-bromo-4-chloro-3-indolyl-phosphate and nitroblue tetrazolium.

Detection of proliferation and apoptosis of adrenal gland cells. Eight-week-old mice were injected intraperitoneally (i.p.) with the thymidine analog 5′-bromo-2′-deoxyuridine (BrdU) (30 mg/g body weight [BW]) every 12 h five times (25). Mice were fully anesthetized and their adrenal glands removed 12 h after the last injection. Incorporated BrdU was detected immunohistochemically using a mouse monoclonal anti-BrdU antibody. The proliferative index was defined as the number of BrdU-positive cells per microscopic field. Five fields per mouse were counted for each of three wild-type (WT) and three ARKO mice.

Cells undergoing apoptosis were identified by digoxigenin labeling of the free 3′OH ends of fragmented DNA by use of terminal deoxynucleotidyltransferase (terminal deoxynucleotidyltransferase-mediated dUTP-biotin nick end labeling [TUNEL] assay). Assays were performed on sections from the same tissue blocks used for BrdU immunohistochemistry. Sections were counterstained with hematoxylin to facilitate cell counting. The fraction of apoptotic cells was defined as the fraction of diaminobenzidine-positive cells per total number of cells. Five fields per mouse were counted for each of three WT and three ARKO mice.

Serum endocrine parameters. A circadian rhythm experiment and dexamethasone suppression tests were performed on 8-week-old male mice as previously described (2). For the circadian rhythm experiment, blood was collected at 08:00 or 18:00 h. For the dexamethasone suppression tests, mice were injected i.p. with different doses of dexamethasone (0, 2, or 5 μg/20 g BW) in 0.3 ml of 0.9% saline. Injections were performed between 08:00 and 08:30 h and blood was collected 6 h later. Mice were fully anesthetized and blood was collected by cardiac puncture. Plasma ACTH and serum corticosterone were measured using radioimmunoassay kits (IRMA; Mitsubishi, Tokyo, Japan) at SRL (Tokyo, Japan), according to the manufacturers' instructions. Measurements were independently duplicated, and interassay variability and buffer dilution were corrected for by using internal correction factors.

RNA extraction and mRNA quantitation. Total mRNA was extracted from pituitary glands with TRIzol (Invitrogen) for reverse transcription-PCR (RT-PCR) and Northern blotting (35). To remove any possible DNA contamination prior to semiquantitative RT-PCR, the DNA was digested with RNase-free DNase. The digested total mRNA (2 μg) was subjected to RT using SuperScript reverse transcriptase (Invitrogen) primed by oligo(dT) primers. After first-strand cDNA synthesis, 1 ml from a 5% reaction mixture was diluted serially (2- to 128-fold). Amplification was performed with *rTaq*DNA polymerase (Takara) using primer pairs for GAPDH as an internal control to allow for concentration estimation (38). Expression levels of transcripts were measured using the standardized cDNA and specific primer pairs. The validity of the PCR products was confirmed by direct sequencing.

Western blot analysis. The lysates of mouse tissue and AtT-20 cells were resolved with sodium dodecyl sulfate-polyacrylamide gel electrophoresis and transferred onto nitrocellulose membranes (15, 39). Membranes were probed with rabbit polyclonal anti-GR antibody (M-20; Santa Cruz Biotechnology) and goat polyclonal anti-β-actin antibody (I-19; Santa Cruz Biotechnology) as an internal control. The blots were visualized using peroxidase-conjugated anti-rabbit antibody and anti-goat antibody, together with an ECL detection kit (Amersham Biosciences). The small interfering RNA analysis used AR and control small interfering RNA (Ambion), and transfection was accomplished with the Lipofectamine 2000 system (Invitrogen).

Luciferase reporter assay. GR promoter regions (upstream regions of exons 1B, 1C, and 2) were cloned by PCR and subcloned into a luciferase reporter gene driven by a tk promoter (tk-luc). PCR primers were as follows: for 1B Fw, 5′-GGCATAGTTAGGCCACTAAAGAGA-3′; for 1B Rv, 5′-GGGAGAAGT TGCAAAGCAGA-3′; for 1C Fw, 5′-CTGGAGCAGCAAATGTCAAG-3′; for 1C Rv, 5′-AGCTCGCAAAATGGAGGAG-3′; for 2 Fw, 5′-GGATCTGGCGT CCTTTTC-3′; and for 2 Rv, 5′-CCACATTATCTCTGATCCGATT-3′.

For the luciferase reporter assay, cultured cells were transfected with the indicated plasmids using the Lipofectamine Plus reagent (Invitrogen) into 24-well plates at 40 to 50% confluence. The total amount of DNA was adjusted by supplementing with empty vector up to 1.0 μg/well. Luciferase activity was determined using a dual luciferase assay system (Promega). As a reference plasmid to normalize the transfection efficiency, 1.5 ng/well of pRL-CMV plasmid (Promega) was cotransfected in all experiments.

Statistical analysis. Values are given as the means ± standard deviations. Comparisons between two groups were made by Student's *t* test. *P* values of <0.05 were accepted as statistically significant.

RESULTS

High serum levels of ACTH and corticosterone in male ARKO mice. The male ARKO ($AR^{L-/Y}$) mice exhibited growth retardation in comparison to WT male mice until 10 weeks of age but then showed catch-up growth over the next few weeks. Thereafter, the male ARKO mice weighed more than the WT mice and developed severe obesity (Fig. 1A) as previously reported (6, 30). Obesity to this extent was not seen for female ARKO ($AR^{L-/L-}$) mice. To identify causes for the late-onset obesity in male ARKO mice, serum endocrine parameters were measured. We found that serum corticosterone levels in male ARKO mice were elevated at 8 weeks of age and became significantly higher at 13 and 20 weeks ($P < 0.05$ and $P < 0.01$, respectively) (Fig. 1B).

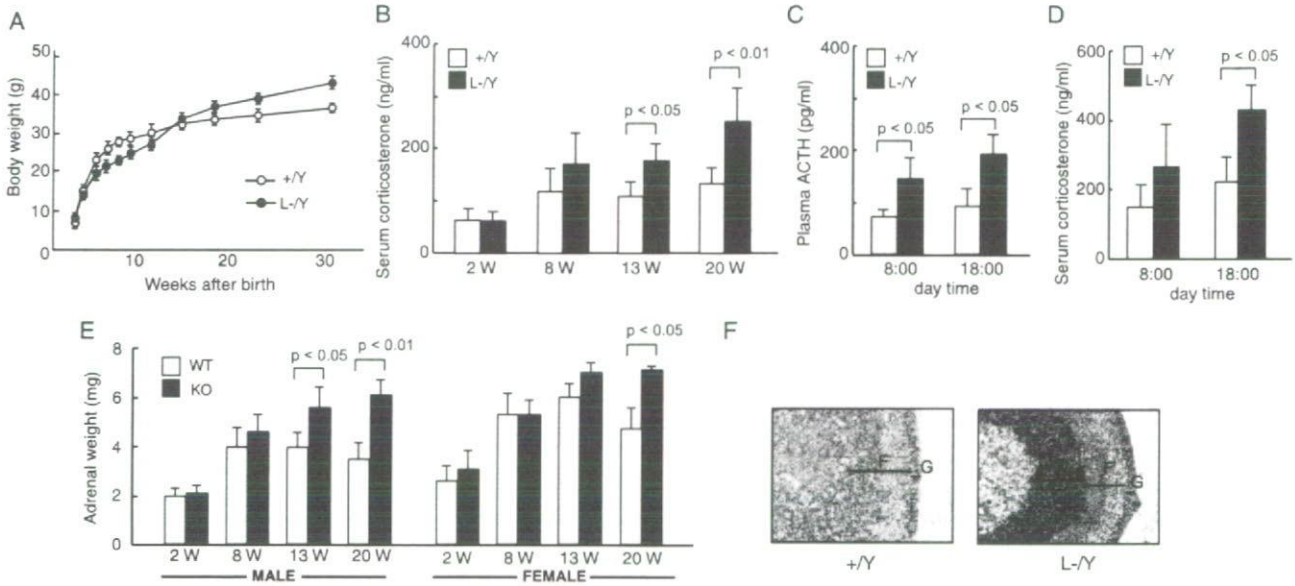

FIG. 1. Hypertrophic adrenal glands with high serum levels of ACTH and corticosterone in ARKO mice. (A) Growth curves of ARKO and WT littermate mice. The floxed AR mice (female, $AR^{L-/L-}$; male, $AR^{L-/Y}$) were crossed with Cre-CMV transgenic mice to generate ARKO male ($AR^{L-/Y}$) and female ($AR^{L-/L-}$) mice (16, 30). (B) Serum corticosterone levels of ARKO and WT mice at 2, 8, 13, and 20 weeks (W) of age. (C) Plasma ACTH levels of ARKO and WT mice measured in the morning (8:00) and evening (18:00). (D) Serum corticosterone levels of ARKO and WT mice in the morning (8:00) and evening (18:00). (E) Adrenal gland weights of male and female ARKO and WT mice at 2, 8, 13, and 20 weeks of age. (F) Histology of ARKO and WT adrenal glands. All sections were stained with hematoxylin and eosin. F, zona fasciculata; G, zona glomerulosa; X, X-zone.

To more carefully examine the hypercorticoid state in male ARKO mice, we measured the serum levels of corticosterone and its upstream hormone ACTH. Measurements were taken both in the morning and in the evening, as these hormones exhibit a circadian rhythm. As expected, the 8-week-old WT and ARKO mice had low levels of both hormones in the morning and higher levels in the evening (Fig. 1C and D). Overall, the ARKO males tended to have high levels of ACTH and corticosterone at any time compared to WT mice. They had significantly high levels of plasma ACTH at both 8:00 and 18:00 and high levels of corticosterone at 18:00 compared to WT mice ($P < 0.05$) (Fig. 1C and D). However, for female ARKO mice, though serum levels of these hormones tended to be higher than in WT littermates, the differences were not statistically significant (data not shown). The obesity seen for these mice was likely the result of their hypercorticoid state, as centripetal obesity is a typical symptom of Cushing's syndrome. In the following experiments, we explored the etiology of the hypercorticoid state in the ARKO mice.

Hypertrophic adrenal glands in ARKO mice. To investigate the hypercorticoid state in the ARKO mice, we first examined the adrenal glands. The adrenal glands in the ARKO males clearly weighed more than the glands of WT mice at 13 weeks of age (Fig. 1E). This coincided with the onset of obesity and the hypercorticoid state. Likewise, in ARKO females, the adrenal glands also increased in size in comparison to what was seen for WT littermate females; however, the growth was not as pronounced as that in ARKO males (Fig. 1E). The adrenal glands of male ARKO mice were then used for subsequent experiments.

The adrenal cortex forms the major part of the gland and is divided into three layers in mammals: the zona glomerulosa, immediately beneath the capsule, followed by the zona fasciculata and the zona reticularis. The zona reticularis is replaced in rodents by the X-zone, which develops prenatally and begins to degenerate at pubertal maturity in males. In mice, corticosterone, the major glucocorticoid in rodents, is produced in the zona fasciculata, while aldosterone, the most potent mineralocorticoid, is formed in the zona glomerulosa. Hematoxylin and eosin staining of adrenal glands in 13-week-old mice revealed that the enlargement of the adrenal glands in ARKO males was caused by cellular hypertrophy of the zona fasciculata as well as by a failure of X-zone (fetal zone) regression (Fig. 1F). Since glucocorticoids are produced in the zona fasciculata, it is likely that the overproduction of corticosterone is the result of the hypertrophy in this area.

Increased proliferation and decreased apoptosis in the adrenal cortex of ARKO males. The failed regression of the X-zone in 13-week-old ARKO males raised the possibility of impaired cell death or decreased apoptosis in the adrenal cortex. Indeed, the percentage of apoptotic cells in the zona fasciculata, detected by TUNEL assay in the ARKO males, was clearly less (19.5%) than that for WT mice (33.1%) (Fig. 2A). When actively proliferating cells of the adrenal glands were counted by BrdU labeling in WT and ARKO males, 2.5 times more BrdU-labeled cells/section were found in ARKO mice. This suggests increased proliferation in the adrenal cortex of ARKO mice (Fig. 2B). Thus, the hypercorticoid state likely results from the overproduction of glucocorticoid by the hypertrophic zona fasciculata. This hypertrophy is caused by chronic exposure to high levels of ACTH.

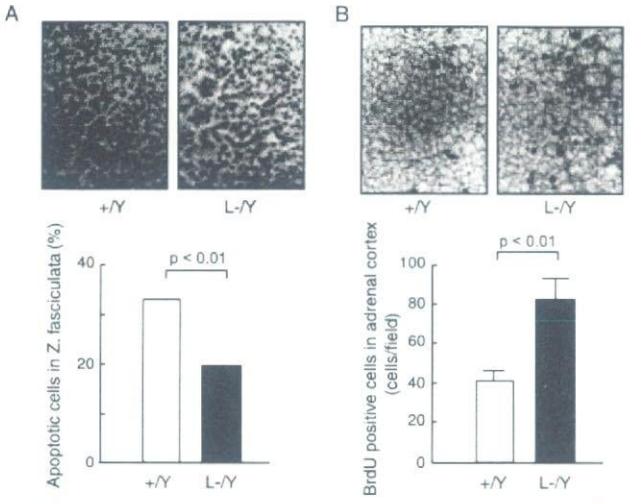

FIG. 2. Increased proliferation and decreased apoptosis in ARKO adrenal glands. (A) Decreased apoptosis in the ARKO adrenal glands. Histogram showing the number of TUNEL-positive cells in the zona fasciculata (Z. fasciculata). (B) Increased proliferation in the ARKO adrenal cortex. Histogram showing the number of BrdU-positive cells.

The HPA negative feedback system for glucocorticoid production is impaired in ARKO males. Glucocorticoid synthesis is regulated by a negative feedback loop via the HPA axis involving CRH and ACTH, produced by the hypothalamus and pituitary glands, respectively. We assessed whether the axis was intact and functioning normally in the ARKO males with a dexamethasone suppression test. As expected, serum corticosterone levels were down-regulated in 8-week-old WT mice 6 hours after i.p. injection of either 2 μg/20 g BW or 5 μg/20 g BW of dexamethasone (Fig. 3A). In ARKO mice, injection with 2 μg/20 g BW of dexamethasone did not suppress the serum levels of corticosterone. However, a dose of 5 μg/20 g BW was effective in lowering the serum levels of corticosterone in ARKO mice (Fig. 3A). This is similar to the high-dose dexamethasone suppression seen for patients with central Cushing's syndrome. Plasma ACTH levels in both the ARKO and WT males were decreased 6 h after dexamethasone injection at both the low and high doses; however, suppression was less sensitive in the ARKO males than in the WT males (Fig. 3B). No statistical difference in ACTH levels was detected between ARKO and WT males in this suppression test.

No overt abnormalities were present in the hypothalami or pituitary glands of ARKO males. The results of the suppression tests suggested that the adrenal hypertrophy of the ARKO males resulted from the hyperfunction of the hypothalami and/or pituitary glands. To address this issue, the hypothalami and pituitary glands of 8-week-old ARKO males were histologically examined. No overt abnormalities were detected in sections of the ARKO mice stained with hematoxylin and eosin (Fig. 4A). Immunohistochemical staining of the pituitary glands demonstrated similar numbers of cells expressing pituitary hormones in WT and ARKO mice (Fig. 4B). AR protein expression was detectable in several types of hormone-producing cells in the WT males but was absent in the ARKO mice (data not shown).

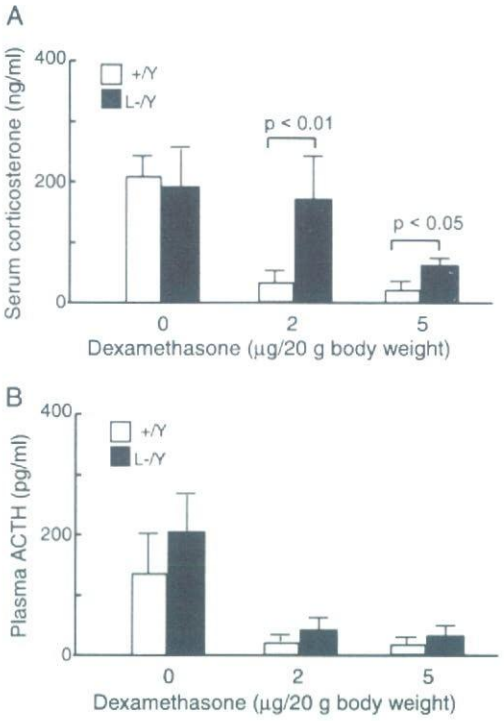

FIG. 3. Impairment of the HPA negative feedback system of glucocorticoid production in ARKO mice. (A) Serum corticosterone levels of ARKO and WT mice in the dexamethasone suppression test. Trunk blood was collected from ARKO and WT mice 6 hours after injection with increasing doses of dexamethasone. (B) Plasma ACTH levels of ARKO and WT mice in the dexamethasone suppression test.

Increased POMC expression and decreased GR expression in the pituitary glands is caused by AR deficiency. To address if hormone production was intact following AR inactivation, we examined the mRNA expression levels of pituitary hormones by RT-PCR. As shown in Fig. 5A, the expression of luteinizing hormone β, follicle-stimulating hormone β, and thyroid-stimulating hormone β, as well as that of the orphan NRs (Nur77 and Nurr1), appeared unaltered by AR deficiency. The POMC mRNA levels, however, were clearly up-regulated in males (Fig. 5A) but not in females (Fig. 5B). The up-regulation of POMC mRNA was confirmed by Northern blot analysis (Fig. 5C). This finding is consistent with the high ACTH levels observed for the ARKO mice. In contrast, pituitary GR expression was decreased at both the mRNA and protein levels (Fig. 5A and D). Decreased GR gene expression in ARKO males was also seen for the spleen but not for the other tested tissues (Fig. 5E), suggesting tissue-specific regulation of GR expression by the AR. Interestingly, a clear decrease in the GR mRNA levels was not detected in the total brain RNA of ARKO males (Fig. 5E). Additionally, there was no alteration in the numbers of GR and CRH immunoreactive cells in the hypothalamic paraventricular nucleus in the male ARKO brain (Fig. 4D). These results suggest that the androgen/AR signaling system affects the negative feedback regulation of glucocorticoid production via pituitary GR expression. This view is further supported by the observation that colocalization of ACTH with the AR and/or GR in the pituitary

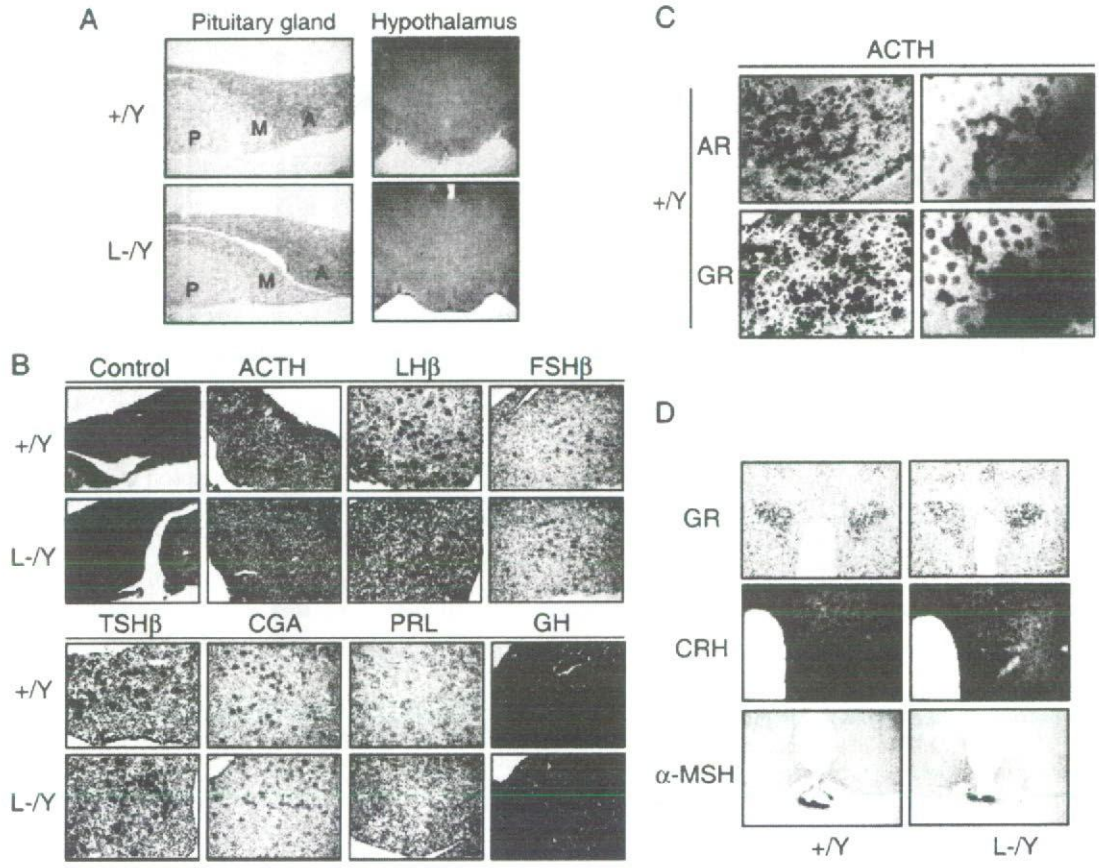

FIG. 4. Histological appearance of the hypothalamus and pituitary gland in ARKO mice. (A) No clear alteration in morphology of the hypothalami or pituitary glands of ARKO mice. Sections of pituitary glands and hypothalami were stained with hematoxylin and eosin. A, anterior lobe; M, intermediate lobe; P, posterior lobe. (B) No overt abnormality in the distribution of cells expressing pituitary hormones in ARKO mice by immunohistochemical staining. LHβ, luteinizing hormone β; FSHβ, follicle-stimulating hormone β; TSHβ, thyroid-stimulating hormone β; CGA, glycoprotein hormone; PRL, prolactin; GH, growth hormone. (C) Pituitary ACTH (black/gray) colocalized with AR (brown) or GR (brown) (left) and its higher magnification (right) in WT mice as detected by immunostaining with specific antibodies. (D) No clear alterations in the GR and CRH (in the paraventricular nucleus) and α-MSH (in the arcuate nucleus) immunoreactive neurons in the hypothalami of ARKO mice.

glands of WT mice was detected by double immunostaining with specific antibodies (Fig. 4C).

Induction of the GR gene by DHT in a pituitary cell line. Finally, to confirm that GR expression levels in the pituitary glands of ARKO mice were reduced, we tested whether DHT induced GR gene expression in cultured cells. DHT treatment of the pituitary cell line AtT-20 for 4 h induced expression of the GR gene (Fig. 6A) and protein (Fig. 6B). Unexpectedly, the expression levels of POMC mRNA (Fig. 6A) and protein (Fig. 6B) were reduced. The AR effect was confirmed following treatment with an AR antagonist (Flutamide) (Fig. 6A and B) and RNA interference (Fig. 6C). Reflecting tissue-specific regulation of GR expression by the AR in intact animals, no response to DHT in the expression levels of either GR or POMC was seen in 3T3-L1 preadipocytes (Fig. 6A to C, lower panels). No consensus androgen response elements or closely related sequences are present up to −3 kb in the GR promoter. However, the intron between exons 1A and 1B of the GR gene (33) was found to counter androgen responsiveness in a transient expression assay in AtT-20 cells (Fig. 6D). This suggests that this element is responsible for androgen-induced GR expression in the pituitary.

DISCUSSION

Hypertrophic and hyperplastic adrenal glands are associated with a hypercorticoid state in male mice deficient for the AR. A hypercorticoid state was observed in sexually mature male mice deficient for the AR. It likely resulted from glucocorticoid overproduction by the hypertrophic and hyperplastic zona fasciculata of the adrenal gland. The ARKO mice demonstrated hyperplasia of the X-zone, which normally regresses by the time sexual maturity is attained (11). TUNEL assays and BrdU labeling confirmed that the hypertrophy and hyperplasia of adrenal glands resulted from decreased apoptosis and increased cell proliferation. Chronic ACTH stimulation causes zona fasciculata cell hypertrophy and hyperplasia, and ACTH is a potent inhibitor of apoptosis in the adrenal cortex (36). Thus, the findings for the ARKO males are consistent with exposure to high levels of ACTH.